Journal of Experimental Botany, Vol. 77, No. 2 pp. 668–685, 2026
https://doi.org/10.1093/jxb/eraf437 Advance Access Publication 3 October 2025

RESEARCH PAPER

Overexpression of the maize 9-lipoxygenase gene *LOX4* confers resistance to *Fusarium verticillioides* via the oxylipin- and jasmonic acid-mediated pathways

Letizia Ottaviani[1], Emilie Montes[2], Thomas Widiez[2], Chiara Dall'Asta[3], Paola Giorni[1], Axel Mithöfer[4], Adriano Marocco[1], and Alessandra Lanubile[1,*]

[1] Department of Sustainable Crop Production, Catholic University of the Sacred Heart, Piacenza 29122, Italy
[2] Laboratoire Reproduction et Développement des Plantes, Univ Lyon, ENS de Lyon, UCB Lyon 1, CNRS, INRAE, Lyon F-69342, France
[3] Department of Food and Drug, University of Parma, Parma 43124, Italy
[4] Research Group Plant Defense Physiology, Max Planck Institute for Chemical Ecology, Jena D-07745, Germany

* Correspondence: alessandra.lanubile@unicatt.it

Received 13 January 2025; Accepted 24 September 2025

Editor: Monica Höfte, University of Ghent, Belgium

Abstract

***Fusarium verticillioides* is a widespread pathogen in cereals that reduces crop yields and poses a threat to food safety by producing the secondary metabolites fumonisins. Maize *lipoxygenase* genes (*LOX*s) are involved in the biosynthesis of oxylipins that function as signals in regulating defense. Previously, we showed that mutation of *LOX4* is associated with susceptibility to *Fusarium verticillioides* in kernels, seedlings, and ears via alterations in both transcript profiles and LOX enzymatic activity. In this current study, we show that *LOX4* overexpression results in enhanced resistance to pathogen infection and fumonisin contamination, substantiating its role in defense. Transcriptomic and lipidomic analyses revealed that *LOX4* overexpression up-regulated expression of 9-LOX genes, thereby increasing the production of 9-oxylipin under fungal infection. The increased expression of jasmonic acid-related genes observed in infected plants was enhanced when *LOX4* was overexpressed, correlating with wider accumulation of jasmonic acid-related metabolites. Our results indicate that *LOX4* is a good target gene for future engineering of cultivars with increased resistance to *F. verticillioides*.**

Keywords: 9-oxylipins, fumonisins, *Fusarium verticillioides*, jasmonic acid, lipidome, lipoxygenase, transcriptome, transgenic maize, *Zea mays*.

Introduction

Fusarium ear rot (FER) caused by *Fusarium verticillioides* (teleomorph *Gibberella moniliformis*) leads to serious losses in yields of maize (*Zea mays*) throughout the world (Zheng *et al.*, 2024). In addition, climate change, and in particular global warming, have consequences on the activity of the fungus and its reproduction cycle, increasing its aggressiveness and production of mycotoxins, in particular fumonisins, to levels above the maximum permitted for food safety (European Commission, 2007;

© The Author(s) 2025. Published by Oxford University Press on behalf of the Society for Experimental Biology.
This is an Open Access article distributed under the terms of the Creative Commons Attribution-NonCommercial License (https://creativecommons.org/licenses/by-nc/4.0/), which permits non-commercial re-use, distribution, and reproduction in any medium, provided the original work is properly cited. For commercial re-use, please contact reprints@oup.com for reprints and translation rights for reprints. All other permissions can be obtained through our RightsLink service via the Permissions link on the article page on our site–for further information please contact journals.permissions@oup.com.

Downloaded from https://academic.oup.com/jxb/article/77/2/668/8271264 by guest on 13 May 2026

Camardo Leggieri *et al.*, 2020). Current disease-management strategies through fungicides and other agronomic practices are often either inadequate or not environmentally sustainable, and hence increasing efforts are being made in breeding to produce maize genotypes with increased resistance to FER and fumonisin contamination (Lanubile *et al.*, 2014a; Logrieco *et al.*, 2021). For instance, generation of null mutants of *FER1* might improve resistance against *F. verticillioides* without any agronomic impairment (Liu *et al.*, 2022). More recently, Ma *et al.* (2023) characterized the cuticular wax biosynthetic gene *WAX2*, and found that mutation of the gene compromises maize resistance to seed and stalk rot, and seedling blight caused by *F. verticillioides*. In contrast, transgenic plants overexpressing *WAX2* show significantly increased immunity to the fungus. Nevertheless, the detailed mechanisms of these resistance traits have not yet been fully elucidated, and further research into these and other ways of improving maize resistance to this fungus is required.

When maize is infected by *F. verticillioides* a cascade of signals within the cell is switched on, leading to the activation of complex local and systemic defense pathways (Lanubile *et al.*, 2017). A key feature of innate immunity is the ability to recognize and respond to potential pathogens in a highly sensitive and specific manner (Monaghan and Zipfel, 2012), and the signals are primarily orchestrated by hormones (Berens *et al.*, 2017). Since defense mechanisms rely on modification and peroxidation of membrane lipids, derived oxylipins have been studied for their possible involvement in plant–pathogen interactions. Oxylipins are active lipid compounds generated through the oxidation of polyunsaturated fatty acids by the action of lipoxygenases (LOXs) (Viswanath *et al.*, 2020). Depending on the regio-specific oxygenation, which can occur at different positions of the hydrocarbon backbone of linoleic (C18:2) or linolenic (C18:3) acid, superfamilies are distinguished as 9-LOXs and 13-LOXs that generate the corresponding 9- and 13-hydroperoxides, respectively (Porta and Rocha-Sosa, 2002; Viswanath *et al.*, 2020). These molecules serve as substrates for seven multi-enzyme branches, involving peroxygenases, divinyl ether synthases, reductases, epoxy alcohol synthases, hydroperoxide lyases, and allene oxide synthases (AOS) and cyclases (AOC), and other subsequent LOX reactions (Berg-Falloure and Kolomiets, 2023). Hydroperoxide lyase activity results in production of green leaf volatiles, divinyl ether synthases produce divinyl ethers such as etherolenic acid, whilst AOS and AOC convert linolenic acid to oxo-phytodienoic acid (OPDA) and jasmonic acid (JA)(Borrego and Kolomiets, 2016).

A total of 13 distinct lipoxygenase genes have been identified in maize, exhibiting diverse functions, localization, and regulatory mechanisms (Borrego and Kolomiets, 2016; Ogunola *et al.*, 2017). Among these, six are responsible for encoding 13-lipoxygenases (*LOX*7–11 and *LOX13*) while *LOX1–5* and *LOX12* encode 9-lipoxygenases (Borrego and Kolomiets, 2016; Ogunola *et al.*, 2017). Meanwhile, the plastidial *LOX6* represents a unique LOX subfamily that has the capability to metabolize fatty acid hydroperoxides produced through the 13-LOX pathway (Gao *et al.*, 2008). The attribution of specific classes of oxylipins to individual *LOX* genes has not been possible so far due to a high degree of redundancy of these genes (Guche *et al.*, 2022).

The antimicrobial and/or antifungal properties of 13-oxylipins, including JA and its conjugates, are well established. Notably, maize JA-deficient mutants of the two oxo-phytodienoate reductase genes *OPR7* and *OPR8* present extreme susceptibility to root-rotting oomycetes, for example *Pythium* spp. (Yan *et al.*, 2012) as well as complete lack of immunity to *F. verticillioides* (Christensen *et al.*, 2014) and *Cochliobolus heterostrophus* (Huang *et al.*, 2023). Increased resistance to *F. verticillioides* stalk rot appears to be associated with JA accumulation and up-regulation of JA-biosynthetic genes in a CO_2-dependent manner (Vaughan *et al.*, 2014).

The contribution of 9-oxylipins to host–pathogen interactions has been less well explored. Functional analysis of maize *lox3* mutants has demonstrated that LOX3 is a susceptibility factor for *F. verticillioides*, *Colletotrichum graminicola*, *C. heterostrophus* (Gao *et al.*, 2007), and *Ustilago maydis* (Pathi *et al.*, 2020), with reduced infection in the mutants. In contrast, the production of *F. verticillioides* conidia is increased when grown on kernels of the *lox4*, *lox5*, and *lox12* mutants, which show decreased contents of JA during the infection (Christensen *et al.*, 2014; Battilani *et al.*, 2018). Our previous studies further highlighted that mutation of *LOX4* compromises resistance to *F. verticillioides* in seedlings (Lanubile *et al.*, 2021a) and ears (Guche *et al.*, 2022), and alters the expression of other *LOX* genes as well as LOX enzymatic activity. In this current study, we used overexpression of *LOX4* to further explore its contribution to FER and seedling-rot resistance mechanisms. We found that the overexpressing lines were significantly less susceptible to the fungus and had lower fumonisin contamination, and showed increased induction of *9-* and *13-LOX* genes together with increases in production of multiple 9-oxylipins and amounts of JA.

Materials and methods

Generation of constructs for transgenic lines

The intron of Arabidopsis *AtFAD2* (*AT3G12120*) under the control of the constitutive cassava vein mosaic virus (*CsVMV*) promoter was used to overexpress the coding sequence (CDS) of *ZmLOX4* (based on the *GRMZM2G109056_T01* or *Zm00001d033624_T01* gene model), followed by the NOS terminator (NOS-ter). The *pCsVMV::ZmLOX4-NOSter* vector (ID# L1781) was generated as follows: the three ENTRY vectors attL4-*pCsVMV*-attR1 (ID# L1054), attL1_ZmLOX4$_{CDS}$_attL2 (ID# L1780), and attR2-NOS-ter_attL3 (ID# M2127; synthetized by Integrated DNA Technologies, https://eu.idtdna.com/page) were assembled with the binary destination vector pBb7m34GW (Karimi *et al.*, 2007) using the MultiSite Gateway Three-Fragment Vector Construction Kit (Invitrogen), according to the manufacturer's instructions.

Downloaded from https://academic.oup.com/jxb/article/77/2/668/8271264 by guest on 13 May 2026

Plant material and genetic transformation

The maize (*Zea mays*) inbred line A188 (Gerdes and Tracy, 1993) was used as the wild-type (WT). The transgenic plants overexpressing *ZmLOX4* (*pCsVMV::ZmLOX4-NOSter*) are referred to as *LOX4*-OE. *Agrobacterium*-mediated transformation was conducted by RDP, Lyon (https://www.ens-lyon.fr/RDP/developpement-de-la-graine/#projBiotec) according to published protocols (Ishida *et al.*, 2007; Fierlej *et al.*, 2022). Two independent T_0 transgenic events (Y381 and Y383) were selected and self-pollinated to obtain plants homozygous for the T-DNA insertion. The presence of the T-DNA was evaluated by PCR on genomic DNA using amplification of the BAR gene, with *GRMZM2G136559/Zm00001eb386680* used as the internal control for the presence and quality of gDNA (primers listed in Supplementary Table S1). T_0 and T_1 plants were grown as described by Doll *et al.* (2019).

Phenotyping of Fusarium ear rot disease

For the phenotyping of Fusarium ear rot (FER), seeds of the WT and two T_2 homozygous seed lots of the transgenic lines *LOX4*-OE1 and *LOX4*-OE2 (derived from Y381 and Y383, respectively) were planted in pots (40 cm diameter, 35 cm height) to produce 30 plants for each line. Plants were grown up in an environmentally controlled chamber with a 16/8 h photoperiod at 28/20 °C (500 µmol m^{-2} s^{-1}, provided by Philips Master TLD 58 W/830 tubes). Heights were measured at week 8 (54 days after sowing; DAS) from the base to the auricles of the youngest fully expanded leaf and at week 11 (75 DAS) from the base to the tip of the panicle. Key agronomic traits of ear length, kernel number per ear, and 100-grain weight were measured at maturity.

The inoculum was prepared from *F. verticillioides* strain ITEM 10027, supplied by the Institute of Sciences of Food Production, National Research Council, Bari, Italy. Conidial suspensions were created as described previously (Lanubile *et al.*, 2021a, 2021b) with a final concentration of 10^6 conidia ml^{-1} and stored at 4 °C before use.

Maize ears were inoculated at the seed milk stage (R3), 15 d after hand-pollination, according to the pin-bar inoculation method (Maschietto *et al.*, 2017. Seeds of control ears were inoculated with sterilized deionized water (mock-inoculated). Inoculated and immediately adjacent seeds were collected at 3 days post-inoculation (dpi) and 7 dpi (Supplementary Fig. S1). At each time-point ~30 seeds from 2–3 different ears were pooled to give five samples per treatment (WT and *LOX4*-OE, control and inoculated). The seeds were ground in liquid nitrogen with a pestle and mortar and stored at −80 °C until further use.

RNA-sequencing and real-time reverse-transcription quantitative (RT-q)PCR) analysis were conducted on seeds collected at 3 dpi using three biological replicates. Hormonal analysis was performed on seeds collected at both 3 dpi and 7 dpi, again using three biological replicates. Lipid analysis was performed on seeds collected at both 3 and 7 dpi, using five biological replicates.

The severity of Fusarium ear rot was evaluated at maturity (45 dpi) using three biological replicates (Supplementary Fig. S1). The percentage of the rotted surface area of the ear was assessed visually using a seven-point scale, as follows: 1, absence of infection; 2, 1–3%; 3. 4–10%; 4, 11–25%; 5, 26–50%; 6, 51–75%; and 7, 76–100% (Maschietto *et al.*, 2017).

Total fumonisin (B_1+B_2+B_3) content was determined on the same ears evaluated for FER severity using VICAM Fumo-V AQUA strips (Waters) as previously described by Guche *et al.* (2022). The strips have a detection limit of 0.2 mg kg^{-1} and a quantitation range from 0–100 mg kg^{-1}.

Phenotyping of Fusarium seedling rot disease

For the phenotyping of Fusarium seedling rot (FSR), the rolled-towel assay (RTA) inoculation method was used to artificially infect mature kernels of each line (Ciasca *et al.*, 2020; Stagnati *et al.*, 2020). Briefly, for each RTA we selected 10 intact seeds of similar size for each of the treatments (infection versus control), and we conducted three replicate RTAs for each treatment × line combination. For each line, a total of six RTAs were carried out, three for the mock and three for inoculated. Seeds were surface-sterilized as previously described (Ciasca *et al.*, 2020) and placed on two moistened towels of germinating paper (Anchor Paper, Saint Paul, MN, USA). The seeds were each inoculated with 100 µl of a conidial suspension (10^6 ml^{-1}) of *F. verticillioides* ITEM 10027 (MPVP 294) prepared as previously reported (Lanubile *et al.*, 2021a, 2021b). The towels were then rolled up and maintained for 7 d at 25 °C in the dark. Controls were prepared as above but treated with 100 µl water. For each seedling, FSR severity, seedling length, and fresh seedling weight were determined. FSR was assessed on each seedling by a visual evaluation of the seedling size and visible colonization of *F. verticillioides* using a scale from 1 to 1–5, as described in Septiani *et al.* (2019). On this scale, 1 corresponds to complete absence of disease symptoms, and five corresponds to entire rotting of the kernel. Coleoptiles at 7 dpi were collected and immediately frozen in liquid nitrogen and stored at −80 °C for further use.

RNA isolation and library preparation

Total RNA was isolated using TRI Reagent® (Sigma-Aldrich) and purified with the RNeasy MinElute Cleanup Kit (Qiagen), according to the manufacturer's instructions (Lanubile *et al.*, 2013). The extracted RNA was quantified using a fluorometric assay (Qubit, ThermoFisher Scientific) and the integrity was checked using the 4150 TapeStation System (Agilent Technologies) as well as gel electrophoresis.

A total of 18 cDNA libraries (three lines × two treatments × three biological replicates) were constructed using a Universal Plus mRNA-Seq Kit (Tecan Genomics) following the manufacturer's instructions and checked with a Qubit fluorometric assay. Libraries were sequenced by IGA-Tech (Udine, Italy) in paired-end 150 bp mode on an Illumina NovaSeq 6000 platform.

Bioinformatic analysis

Paired-end reads were demultiplexed, processed for adapter masking and trimmed using Illumina BCL Convert v3.9.3. The quality of trimmed reads was assessed using the ERNE v2 software (Del Fabbro *et al.*, 2013). High-quality reads were mapped against the *Zea mays* B73 GRAMENE_v4 genome with STAR read aligner (Dobin *et al.*, 2013). Assembling and quantitation of full-length transcripts representing multiple spliced variants for each gene locus was carried out using Stringtie (Pertea *et al.*, 2015) and gene expression values were quantified as counts per million (CPM). Pairwise differential expression analysis was carried out with DESeq2 (Anders and Huber, 2010; Love *et al.*, 2014) using a Wald test performed to verify whether there were differentially expressed genes (DEGs) between two sample groups. A gene was considered differentially expressed if the adjusted *P*-value was <0.05, regardless the fold-change.

Venn diagrams of the DEGs were constructed using the Bioinformatics & Evolutionary Genomics web tool (https://bioinformatics.psb.ugent.be/webtools/Venn/). Graphs were plotted using the *ggplot2* and *heatmap.2* packages in R (www.r-project.org; https://cran.r-project.org/web/packages/gplots/index.html).

Gene Ontology and KEGG analyses

Functional annotation was obtained through API using swagger for Gramene release 67 (https://data.gramene.org/v67/docs/?url=/v67/swagger) in the Python environment. Gene Ontology (GO) and KEGG pathway enrichment for each set of DEGs were analysed using ShinyGO v0.80 (http://bioinformatics.sdstate.edu/go/) run with default parameters (Ge *et al.*, 2020; Kanehisa *et al.*, 2021), and results were

Downloaded from https://academic.oup.com/jxb/article/77/2/668/8271264 by guest on 13 May 2026

visualized with Pathview (Luo and Brouwer, 2013). Enrichment *P*-values were obtained using the hypergeometric test. To correct for multiple testing, the false-discovery rate (FDR) was calculated using the Benjamini–Hochberg method. Pathways were considered enriched if the FDR-corrected *P*-values was <0.05.

Real-time RT-qPCR expression analysis

To verify the overexpression of *LOX4* in the T_2 *LOX4*-OE homozygous plants, tissues at different developmental stages were collected from the WT and transgenic lines and tested by real-time RT-qPCR using 2× iQ SYBR Green Supermix and a CFX-96 device (both Bio-Rad). In detail, we sampled the coleoptile and the radicle at 7 DAS, the tip of the seventh leaf at 42 DAS, the tip of the tassel at 55 DAS, and the silks at 60 DAS from three replicate plants, and 1 µg of total RNA was reverse-transcribed to cDNA using an iScript cDNA Synthesis Kit (Bio-Rad) according to the manufacturer's protocol. Then 20 ng of single-strand cDNA, as determined by fluorometric assay (Qubit, ThermoFisher Scientific), were employed for RT-qPCR with the following thermal-cycling conditions: 95 °C for 2 min and 35 cycles at 95 °C 10 s, 62 °C for 30 s, followed by a melting-curve analysis. Specific primers for the *LOX4* endogene and *LOX4*-OE transgene are listed in Supplementary Table S1 (Guche *et al.*, 2022). Two technical repeats were performed for each biological replicate. Relative expression was normalized to the reference gene *β-actin* and fold-change (FC) values were calculated using the $2^{-\Delta\Delta CT}$ method (Schmittgen and Livak, 2008). The Cq values of *actin* gene under all experimental conditions (mock/inoculated and tissues) are given in Supplementary Table S2.

RT-qPCR was also conducted for validation of RNA-seq data on seeds collected at 3 dpi, with the following conditions: 95 °C for 3 min and 40 cycles at 95 °C 15 s, 57–63 °C for 30 s, followed by a melting-curve analysis (Maschietto *et al.*, 2015; Lanubile *et al.*, 2021a). Gene-specific primers are listed in Supplementary Table S1.

The growth of the fungus was quantified using the copy number of *F. verticillioides calmodulin* transcripts as detected by RT-qPCR in inoculated coleoptiles collected at 7 dpi in the Fusarium seedling rot phenotyping assay. The primer pairs were designed within a conserved region positioned between nucleotides 13 and 162 of the *calmodulin* sequence (Maschietto *et al.*, 2016; Lanubile *et al.*, 2021b) (Supplementary Table S1). The RT-qPCR thermal cycling conditions were the same as described for the validation of RNA-seq data considering an annealing temperature of 60 °C. The *calmodulin* copy number was related to the quantity of cDNA (ng) obtained from seed tissues and determined based on the linear regression calculated to the Bio-Rad technical manual. Fungal cDNA (20 ng) was serially diluted (1:1, 1:5, $1:5^2$, $1:5^3$, $1:5^4$, $1:5^5$) in sterile water and 20 ng of each seed cDNA sample was compared to the dilution standard curve to determine fungal cDNA copy number.

Hormonal analysis

Seeds were freeze-dried at −80 °C and samples of ∼30 mg were extracted according to Pimentel *et al.* (2021) in order to analyse the contents of salicylic acid (SA), 12-oxo-phytodienoic acid (*cis*-OPDA), jasmonic acid (JA), 12-hydroxyjasmonic acid (OH-JA), the jasmonoyl isoleucine conjugate (JA-Ile), hydroxyjasmonoyl-isoleucine (OH-JA-Ile), and dicarboxyjasmonoyl-isoleucine (COOH-JA-Ile) by LC–MS/MS. Briefly, seeds were extracted in 1.5 ml methanol containing internal standards of 40 ng D4-SA (Sigma-Aldrich), 60 ng D6-JA, and 12 ng D6-JA-Ile (both HPC Standards GmbH, Cunnersdorf, Germany). The homogenate was mixed for 30 min, debris was removed by centrifugation (20 min at 4 °C at 15 000 *g*), and the supernatant was collected. The homogenate was re-extracted with 500 µl methanol, centrifuged, and the supernatants were pooled. The combined extracts were evaporated under reduced pressure at 30 °C and dissolved in 500 µl methanol. Determination of phytohormones was performed by LC–MS/MS using an LC-TripleQuad-MS system according to Heyer *et al.* (2018) on an Agilent 1260 series HPLC system equipped with an Agilent Zorbax Eclipse XDB-C18 column (50×4.6 mm, 1.8 µm) and coupled to a tandem MS API6500 (SCIEX) with a turbo spray ion source operated in negative ionization mode. The ion spray voltage was maintained at −4500 eV. The turbo gas temperature was set at 700 °C. Nebulizing gas was set at 60 psi, curtain gas at 25 psi, the heating gas at 60 psi, and collision gas at 7 psi. Multiple reaction monitoring was used to monitor fragmentations of analyte parent ions to product ions as described in detail by Heyer *et al.* (2018). Compounds were quantified by comparison of the sample peak areas to the peak area of the corresponding internal standards: the individual response factors (RF) were determined by analysing a mixture of the particular compounds with either D6-JA-Ile (for JA-Ile derivatives; RFs all 1.0), D4-SA (for SA-glucoside; RF 1.0), or D6-JA (for OPDA; RF 0.5) at the same concentrations (Dávila-Lara *et al.*, 2021).

Untargeted lipidomics

Oxylipins were mapped and semi-quantified using an untargeted lipidomics approach previously developed and applied by our group (Rubert *et al.*, 2017; Righetti *et al.*, 2021, 2024). The linoleic acid oxylipins MaxSpec® LC-MS Mixture was purchased from Cayman (Vinci-Biochem, Firenze, Italy).

Seeds were extracted according to a scaled-down procedure as reported by Rubert *et al.* (2017). Briefly, 100 mg of finely ground sample was weighed into a 2 ml Eppendorf tube and 1 ml of a cold mixture composed of dichloromethane and methanol (50:50, v/v) was added as an extraction solvent. The mixture was vortexed for 15 min at 240 s min^{-1} and centrifuged at ∼2000 *g* and 4 °C for 10 min. Afterwards, 200 µl of the upper phase was transferred to a glass vial and dried under a gentle nitrogen flow. Finally, the sample was reconstituted in 1 ml of a 2-propanol/methanol/water mixture (65:30:5, v/v/v) before injection. Five replicate samples were used.

Separation and identification were achieved on an Acquity I-class ultra-performance LC separation system coupled to a Vion IMS QTOF mass spectrometer (Waters) equipped with an electrospray ionization interface. Samples (1 µl) were injected and chromatographically separated using a reversed-phase C18 BEH Acquity column (2.1×100 mm, 1.7 µm particle size) (Waters). Gradient elution was set according to Righetti *et al.* (2021). The MS data were collected in negative electrospray mode over the mass range of m/z 100–1100. Source settings were maintained using a capillary voltage of 2.5 kV, a source temperature of 120 °C, a desolvation temperature of 500 °C, and a desolvation gas flow of 1000 l h^{-1}. The TOF analyser was operated in sensitivity mode, and data were acquired using a High-Definition MS^E, which is a data-independent approach coupled with ion mobility. The optimized ion mobility settings included a nitrogen flow rate of 90 ml min^{-1} (3.2 mbar), a wave velocity of 650 m s^{-1}, and a wave height of 40 V. The TOF was also calibrated prior to data acquisition and covered the m/z range 151–1013. TOF and collision cross-section calibrations were performed for both positive- and negative-ion modes. Data acquisition was conducted using the Waters UNIFI 1.8 software.

A randomized injection sequence was applied to avoid any possible time-dependent changes during the ultra-HPLC-Q-TOF-MS analysis, which could result in false clustering. The quality-control sample, prepared by pooling an aliquot of the extract from each sample, was injected at the beginning of the sequence and after every 10 sample injections.

Data processing and compound annotation were conducted using Progenesis QI Informatics (Nonlinear Dynamics, Newcastle, UK). Briefly, each ultra-HPLC-MS run was imported as an ion-intensity map, including m/z (range 100–1100) and retention time, that were then aligned in the retention-time direction (0.5–16 min). Principal component analysis (PCA) with Pareto scaling was performed to check the quality of the raw data and then the variables were filtered, retaining

Downloaded from https://academic.oup.com/jxb/article/77/2/668/8271264 by guest on 13 May 2026

entities with coefficients of variation lower than 30% across the quality controls.

The data set was then exported into MetaboAnalyst 6.0, log-transformed, and Pareto-scaled before evaluating the quality of the unsupervised and supervised models. PCA was performed to assess the natural sample grouping. Significant variables were selected according to a FDR-corrected value of $P<0.01$.

Annotation was performed using the Progenesis Metascope tool with an in-house library of plant oxylipins obtained from KEGG analysis and LIPID MAPS (https://www.lipidmaps.org/). The identification was assigned at level I or level II following the annotation levels of the Metabolomic Standard Initiative (Schymanski *et al.*, 2014).

Fungal growth bioassays

The ITEM 10027 strain of *F. verticillioides* was inoculated on potato dextrose agar plates and incubated at 25 °C for 14 d. The plates were then washed with sterile distilled water and the spores were collected and adjusted to a concentration of 10^6 conidia ml^{-1}. This solution was then used as inoculum for a 96-well plate to determine the growth of *F. verticillioides* in the presence of oxylipins. Five different oxylipins were tested: 12-oxo-phytodienoic acid (CAS: 85551-10-6), jasmonic acid (CAS: 77026-92-7), traumatic acid (CAS: 6402-36-4), and 9-oxononanoic acid (CAS: 2553-17-5; all Cayman Chemical Company, Ann Arbor, MI, USA), and *trans*-2-hexenal (CAS: 6728-26-3; Glentham Life Sciences Ltd, Corsham, UK). Each was tested at a final concentration of 100 μM in 200 μl of liquid medium per well, with 12 replicate wells for each condition. Growth medium without the tested oxylipin was included as a negative control. Fungal growth was monitored using an Agilent BioTek 800 TS absorbance reader over a period of 7 d at 25 °C. Optical density readings were taken every 11 min at a wavelength of 405 nm (OD_{405}). Prior to each automated reading, the plates were shaken at a linear frequency of 567 cpm for 10 s, and a total of 917 readings per well was obtained.

Fungal growth over the 7 d period was assessed by calculating the area under the growth curve (AUGC):

$$AUGC = \sum[(OD_{i+1} + OD_i)/2] \times (t_{i+1} - t_i)$$

where OD_{i+1} and OD_i are the OD_{405} values at times t_{i+1} and t_i, respectively (i.e. AUGC is the sum of the mean OD_{405} values across all the 11-min intervals). To assess the variability in the AUGC as affected by oxylipin treatment, coefficients of variation (CV, %) were calculated for each condition as 100×SD/mean, where a higher CV indicates a greater variability. Statistical analyses and plots were performed using R (www.r-project.org).

Statistical analysis

One- and two-way ANOVA and Tukey's HSD tests were performed to determine significant differences using SPSS statistics 27.

Results

Characterization of the *LOX4*-overexpressing lines

To explore the impact of overexpression of *LOX4* on maize responses to *F. verticillioides* infection, the *CsVMV* promoter was used to drive its expression in the A188 wild type (WT) background (Fig. 1A). Two independent transgenic lines were selected and named as *LOX4*-OE1 and *LOX4*-OE2. RNA-seq results from kernels at the milk stage showed that expression levels were ~69 and ~81 times higher compared with the WT kernels for *LOX4*-OE1 and *LOX4*-OE2, respectively (Fig. 1B). The expression of the *LOX4* endogene and *LOX4*-OE transgene was measured by RT-qPCR in the coleoptile, radicle, leaf, tassel, and silks of the WT and the two transgenic lines (Fig. 1C). The results confirmed the presence of the transgene only in the *LOX4*-OE lines in all the tissues, accompanied by marked overexpression in both the OE lines, with significantly higher expression in OE2 (126.5–408.9-fold) compared with OE1 (4.8–24.6-fold). No substantial differences were observed for the transcript accumulation of the endogene among the three genotypes, except for the silks where it was 4- and 16-fold lower in the OE1 and OE2 lines, respectively, as compared with the WT.

LOX4-overexpression reduces Fusarium ear and seedling rot diseases

Previous studies have shown that mutation of *LOX4* impairs maize resistance to both FER and FSR diseases (Lanubile *et al.*, 2021a; Guche *et al.*, 2022), so we assessed their severity in ears and seedlings in the *LOX4*-overexpressing lines.

Flowering time was recorded during the phenotyping of FER, and we found that male flowering started between 64–68 DAS for the WT plants and 68–72 DAS for the OE lines. Plant heights were measured at weeks 8 and 11. At week 8, a small but significant difference was seen between the OE1 and OE2 lines (53.5 cm and 44.2 cm, respectively; Supplementary Figs S2, 3A) but neither line was different from the WT. At week 11, there were no differences between any of the genotypes (Supplementary Fig. S3B). Ear length, kernel number per ear, and 100-grain weight at maturity also showed no significant differences among the genotypes (Supplementary Fig. S3C–E).

Severity symptoms for FER on the ear itself were limited to the inoculation point in the two OE lines (Fig. 2A), and quantification indicated that the OE1 and OE2 lines had infection scores of ~2.8 and 3.2, respectively, compared with ~6 for the WT (Fig. 2B). The inoculated WT kernels appeared more seriously injured by the pathogen with clearly visible rotting also having progressed to adjacent kernels.

The results for total fumonisin ($B_1+B_2+B_3$) content in the ears were in line with the FER phenotyping (Fig. 2C), with values significantly higher in the WT (~3,387 ppb) compared with the OE1 and OE2 lines (1,188 ppb and 614 ppb, respectively). These results indicated that *LOX4* was positively associated with limitation of both the spread of the disease and the presence of *Fusarium* mycotoxins in the kernels.

Seedlings of the WT and the two OE lines also showed distinct types of response to FSR, as determined using rolled-towel assays (RTAs). Both the overexpressing lines were significantly less susceptible to *F. verticillioides*, displaying FSR severity scores of ~3 and ~2.4 for OE1 and OE2, respectively, compared with 3.5 for the WT (Fig. 2D, E). Consistent with this, absolute quantification of the activity of the *F. verticillioides calmodulin* gene by RT-qPCR indicated that the

Downloaded from https://academic.oup.com/jxb/article/77/2/668/8271264 by guest on 13 May 2026

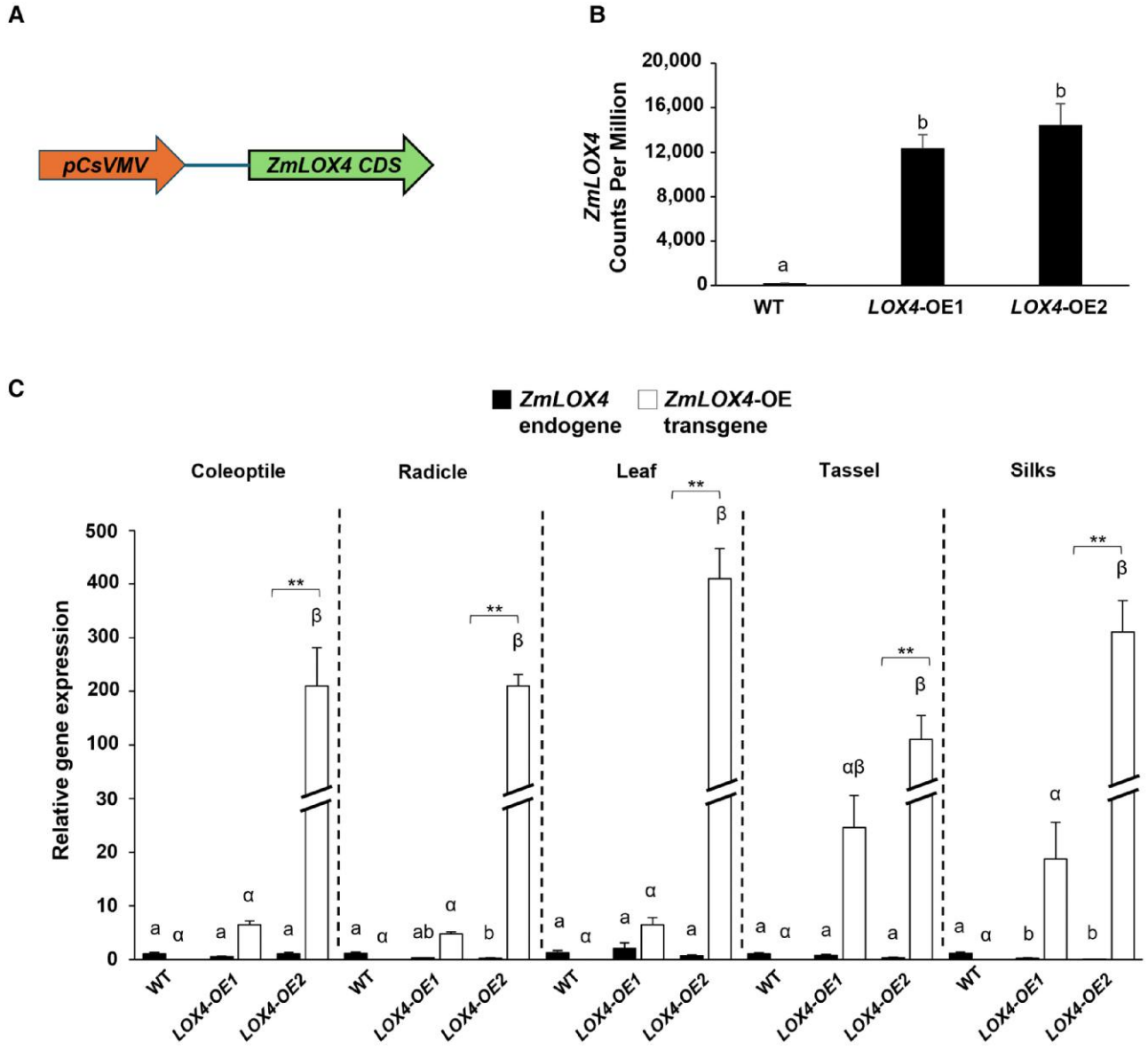


Fig. 1. Overexpression of *LOX4* in maize (A) Schematic diagram of the *ZmLOX4*-overexpression (OE) cassette under the control of the Cassava vein mosaic virus (*CsVMV*) promoter. CDS, coding sequence. (B) *ZmLOX4* transcript abundance as determined by RNA-seq analysis in the kernels of the wild-type A188 cultivar (WT) and two independent *LOX4*-OE lines. (C) Relative expression of the *ZmLOX4* endogene and *ZmLOX4*-OE transgene in the three genotypes in the coleoptile and radicle at 7 days after sowing (DAS), in the tip of the seventh leaf at 42 DAS, in the tip of the tassel at 55 DAS, and silks at 60 DAS. Data are means (±SD), n=3. Different letters indicate significant differences among means as determined using one-way ANOVA followed by Tukey's HSD test (P<0.05); in (C) Greek letters are used for differences for the transgene. Significant differences between the endogene and transgene within a genotype were determined using two-way ANOVA: $^{**}P \leq 0.01$.

coleoptile tissues of the OE lines were less colonized by the fungus compared with the WT, with a transcript copy number ~17 times lower (Fig. 2F). In line with these results, seedling weight and length were less negatively affected by *F. verticillioides* in the OE lines than the WT (except for seedling length in OE2; Supplementary Fig. S4), suggesting better performances of the transgenic lines in terms of disease resistance and seedling growth.

Overall, these results demonstrates that enhanced expression of *LOX4* increased resistance to *F. verticillioides*.

Transcriptome analysis of mock and inoculated kernels

RNA-sequencing of libraries obtained from maize kernels belonging to the WT and OE lines either mock-inoculated or at 3 dpi with *F. verticillioides* produced 578, 600, 000 and 436, 500, 000 paired-end 150 bp reads, respectively, corresponding

Downloaded from https://academic.oup.com/jxb/article/77/2/668/8271264 by guest on 13 May 2026

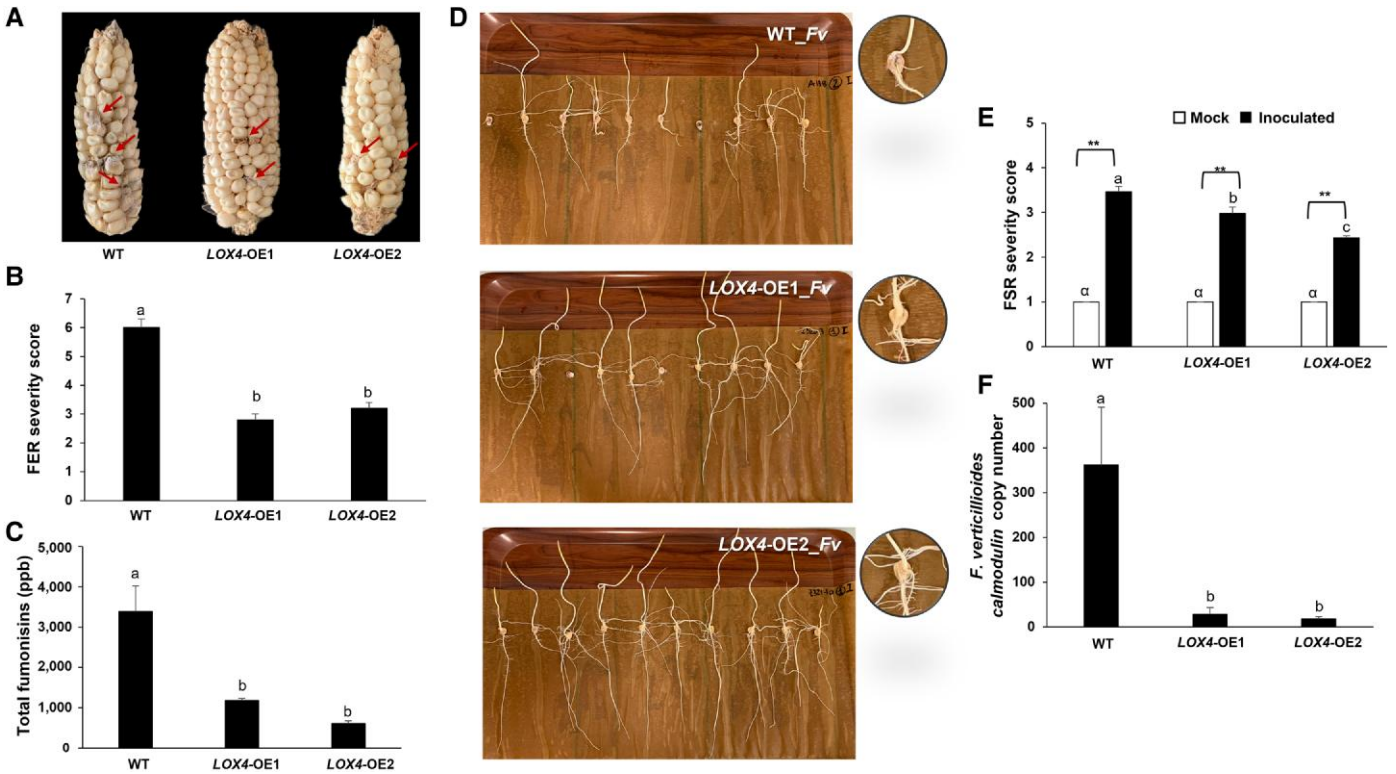


Fig. 2. Phenotyping of Fusarium ear rot (FER) and Fusarium seedling rot (FSR) diseases caused by *F. verticillioides* in the maize A188 wild type (WT) and two *LOX4*-overexpressing lines (OE1, OE2) at maturity. (A) Representative images of FER disease. The arrows indicate the inoculation points. (B) Quantification of FER disease severity in inoculated ears on a seven-point scale, where 1 represents no disease and 7 represents up to 100% of ear rotting. (C) Concentration of total fumonisins (B_1+B_2+B_3) in the kernels. (D) Representative images of FSR disease on 7-day-old inoculated seedlings, and (E) quantification of disease severity in mock controls and inoculated seedlings on a five-point scale, where 1 represents no disease and 5 represents rotting of the entire kernel. (F) Quantification of disease in inoculated seedlings by *F. verticillioides calmodulin* copy number. Data are means (±SD) of n=3 biological replicates, except for (E) where n=3 independent experiments, each consisting of 10 seedlings per treatment. Different letters indicate significant differences among means as determined using one-way ANOVA followed by Tukey's HSD test (P<0.05); in (E) Greek letters are used for differences among the mock treatments. Significant differences between the mock and inoculated treatments within a genotype were determined using two-way ANOVA: $^{**}P \leq 0.01$.

to ~115.7 and ~87.3 Gbps (Supplementary Table S3). On average, ~66% of the total reads mapped to the maize inbred line B73 v4 reference genome sequence, with most of the reads mapping to exons (~82.2%), followed by UTRs (~8.4%), intergenic regions (~7.8%), and introns (~1.6%; Supplementary Fig. S5). From the gene annotation on the B73 reference genome a total of 29,516 genes was obtained (Supplementary Table S4).

Expression profiles of the inoculated WT and OE lines were compared with the corresponding mock-inoculated samples, whilst intergenotype differences were examined by comparing mock-inoculated WT and OE lines. This transcriptome analysis revealed a total of 9,618 DEGs, grouped in six clusters based on their expression profiles (Supplementary Fig. S6).

Effects of *LOX4*-overexpression on the transcriptome in the absence of infection

Constitutive differences between the two transgenic OE lines and the WT were investigated by comparing mock-inoculated samples (Supplementary Fig. S6, clusters I–III). Differential expression analysis revealed 1,809 significant DEGs for OE1 versus WT (871 up- and 938 down-regulated), 2,712 DEGs for OE2 versus WT (1,062 up and 1,650 down), and 587 DEGs for OE2 versus OE1 (210 up and 377 down) (Fig. 3A, B; Supplementary Table S5). There were 681 DEGs that were uniquely expressed in the comparison OE1 versus WT, 1,502 in the comparison OE2 versus WT, and 254 in the comparison OE2 versus OE1, with 23 being common to all comparisons. To investigate the function of transcripts differentially expressed at a basal level and potentially influenced by *LOX4*-overexpression, a GO enrichment analysis was carried out (Supplementary Table S5; Supplementary Figs S7, S8). The top 50 GO terms with the smallest FDR values that were significantly enriched in the category 'Biological Process' (BP) are shown at Supplementary Fig. S7. In the three comparisons, most of the BP terms referred to DNA replication, transcription, and translation processes, such as 'Double-strand break repair via break-induced replication', 'Mitotic DNA replication', 'Protein complex oligomerization', and 'Response to unfolded protein'. Additional pathways were

Downloaded from https://academic.oup.com/jxb/article/77/2/668/8271264 by guest on 13 May 2026

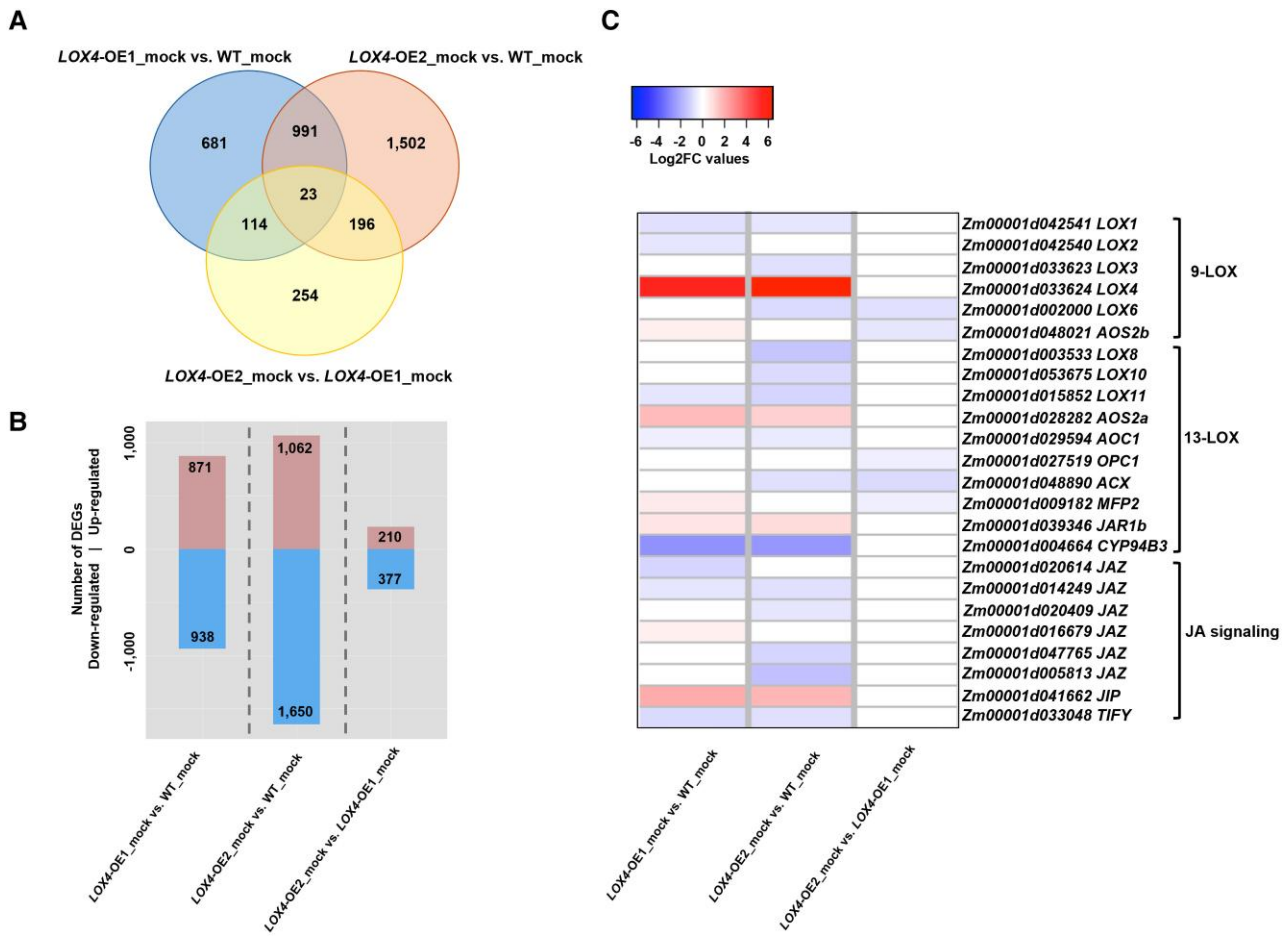


Fig. 3. RNA-sequencing analysis of the maize A188 wild type (WT) and two *LOX4*-overexpressing lines (OE1, OE2) in the absence of disease (mock inoculation). (A) Venn diagram of the numbers of differentially expressed genes (DEGs) in the different comparisons among the genotypes. (B) Numbers of up- and down-regulated DEGs in the three comparisons. (C) Heat-map showing the expression patterns of genes involved in the 9- and 13-LOX pathways together with the jasmonic acid (JA)-mediated signaling pathway in the three comparisons.

associated with primary metabolism ('L-phenylalanine catabolic process', 'Erythrose 4-phosphate/phosphoenolpyruvate family amino acid catabolic', 'Regulation of ATP dependent activity', and 'Tyrosine metabolic process') as well as with the response to several environmental stresses ('Response to xenobiotic stimulus', 'Cellular response to red or far red light', Response to heat', and 'Response to salt stress'). Interestingly, the comparison between the strongest *LOX4*-overexpressing line (OE2) with WT showed significant enrichment of the terms 'Oxylipin metabolic process', 'Oxylipin biosynthetic process', and 'Regulation of jasmonic acid mediated signaling pathway' (Supplementary Fig. S7B).

KEGG pathway analysis was also conducted for the three comparisons and showed many common significantly enriched pathways, such as 'DNA replication', 'Circadian rhythm plant', 'Glycolysis and Gluconeogenesis', and 'MAPK signaling pathway plant' (Supplementary Fig. S8). Notably, and in line with the GO analysis, the 'linoleic acid metabolism' pathway was highly enriched only in the comparison OE2 versus WT.

Focusing on key DEGs involved in the 9- and 13-LOX pathways together with those in the jasmonic acid-mediated signaling pathway, a total of 24 genes were observed in the three comparisons, most of them down-regulated in the comparisons of the two OE lines versus WT (Fig. 3C; Supplementary Table S5). This suggested that at the basal level the overexpression of *LOX4* reshaped the expression of other genes implicated in the production of 9-oxylipins and jasmonates.

LOX4-overexpression amplifies the transcriptome response to inoculation

To identify the crucial genes implicated in the maize–*F. verticillioides* interaction and potentially modulated by *LOX4*-derived oxylipins, we examined DEGs in the two OE lines and the WT between samples with fungal inoculation and with mock inoculation at 3 dpi (Supplementary Fig. S6, clusters IV–VI; see Supplementary Table S6 for full list). A total

Downloaded from https://academic.oup.com/jxb/article/77/2/668/8271264 by guest on 13 May 2026

of 3,379 significant DEGs were found for the WT (2,472 up- and 907 down-regulated), 4,434 for OE1 (2,850 up and 1,584 down), and 7179 for OE2 (4,633 up and 2,546 down) (Fig. 4A, B). The common DEGs (1,902) represented the largest proportion (~42%) among the three comparisons, suggesting an important conserved core response to pathogen inoculation. There were 600 genes uniquely modulated in the WT genotype, whilst there were 1,205 and 3,349 DEGs specifically identified in the OE1 and OE2 lines, respectively.

GO enrichment and KEGG pathway analyses were conducted to get an overview of DEGs potentially relevant to FER resistance (Fig. 4C, D; Supplementary Table S7). The majority of significantly enriched BP terms and KEGG pathways ($P<0.05$) were common among the three comparisons and multiple processes related to defense response were identified. For the GO terms, these included 'Defense response', 'Response to fungus', 'Regulation of JA mediated signaling pathway', 'Oxylipin metabolic process', 'Oxylipin biosynthetic process', 'Cell wall macromolecule metabolic process', 'Cell wall macromolecule catabolic process', 'Chitin metabolic process', 'Chitin catabolic process', and 'Lignin metabolic process' (Fig. 4C). For the KEGG pathways, these included 'Plant–pathogen interaction', 'Linoleic acid metabolism', 'Alpha-linolenic acid metabolism', 'Biosynthesis of secondary metabolites', 'Phenylpropanoid biosynthesis', 'Flavonoid biosynthesis', 'Terpenoid backbone biosynthesis', and 'Diterpenoid biosynthesis' (Fig. 4D). Intriguingly, the GO terms 'Response to superoxide', 'Response to oxygen radical', 'Removal of superoxide radicals', and 'Cellular response to superoxide' were found only in the comparisons OE1–*Fv* versus OE1–mock and OE2–*Fv* versus OE2–mock (Fig. 4C). Focusing on these pathways, seven genes were detected overall, all of which were up-regulated (*Zm00001d029170*, *Zm00001d002611*, *Zm00001d022505*, *Zm00001d047479*, *Zm00001d053118*, *Zm00001d037429*, and *Zm00001d009990*), with *Zm00001d029170* encoding a superoxide dismutase having the highest CPM values with infection (2,121.6 and 1,851.6 for *OE1* and *OE2*, respectively) and $\log_2$FC values of 1.11 and 0.65 for OE1 and OE2, respectively (Supplementary Tables S6, S7).

When the common defense-related categories were examined more closely, important differences in the level of induction were observed between the WT and the two OE lines. For instance, analysis of the modulation patterns of all DEGs associated with the 9- and 13-LOX pathways along with the JA-mediated signaling pathway indicated increased expression of oxylipin and JA biosynthesis genes in all three genotypes, but to a higher extent in the OE lines (Supplementary Fig. 9; Supplementary Table S6). Notably, the *LOX4* was not differentially expressed in the two transgenic lines following *F. verticillioides* inoculation; however, the mean CPM values following infection were 10, 116.4 and 11, 470.1 for the OE1 and OE2 lines, respectively, whereas the values for the WT were ~8 times lower (1216.31; Supplementary Tables S4, S6). For the categories related to oxylipin and JA, the number of DEGs and their mean fold-change levels were directly proportional to the *LOX4* counts, with the OE2 line having 57 DEGs (52 up- and five down-regulated) and a mean $\log_2$FC value of 1.7, the OE1 line having 45 DEGs (39 up and six down) and a mean $\log_2$FC value of 1.4, and the WT having 41 DEGs (34 up and seven down) and a mean $\log_2$FC value of 1.2 (Supplementary Fig. S9; Supplementary Table S6). The gene with the highest CPM values under infection was *Zm00001d018487*, encoding acetyl C, with values of 6,862.1, 7,101.2, and 7,149.5 in the WT, OE1, and OE2 lines, respectively.

Similar results were detected for the GO category 'Defense response' (Fig. 4C). This term was highly enriched by up-regulated DEGs in all three genotypes, but the OE2 line showed the highest number (102 versus 70 in the WT and *OE2*), with a mean $\log_2$FC value of 3.2 compared with 2.20 for OE1 and 1.8 for the WT (Supplementary Tables S6, S7). The highest expression levels under infection were observed for *Zm00001d003190*, encoding a chitinase, with CPM values of 85, 004.5, 53, 574.6, and 39, 842.0 in OE2, OE1, and WT, respectively.

Comparable findings were observed for the KEGG pathway 'Biosynthesis of secondary metabolites' and associated ones such as 'Phenylpropanoid, Flavonoid and Terpenoid/Diterpenoid biosynthesis' (Fig. 4D). The two OE lines always showed a higher number of DEGs and mean CPM values under infection compared with the WT, more markedly in the OE2 line. As an example, for the category 'Biosynthesis of secondary metabolites', there were 176 genes that were differentially modulated (mostly up-regulated) in the WT, whereas the corresponding numbers in the OE1 and OE2 lines were 188 and 283, respectively; the mean CPM values under infection were 1,547.8, 1,598.6, and 1,689.0 for the WT, OE1, and OE2, respectively (Supplementary Tables S6, S7).

Thus, the transcripts of a considerable number of genes were found to be commonly modulated by the fungus in all the comparisons, but the overexpression of *LOX4* resulted in an enhanced response in the two transgenic lines, mainly affecting defense-associated genes.

To confirm the reliability of RNA-seq data, 12 genes were selected for RT-qPCR validation, four of which were involved in the 9- and 13-LOX pathways (*LOX2*, *Zm00001d042540*; *LOX3*, *Zm00001d033623*; *AOS2b*, *Zm00001d048021*; and *ACX*, *Zm00001d045251*). The comparison between the two techniques showed substantial agreement for 11 genes that were differentially expressed before and after *F. verticillioides* inoculation (Supplementary Fig. S10). Consistent with the sequencing data, the transgenic lines generally displayed enhanced modulation levels, and this trend followed the increased *LOX4* expression levels.

Effects of *LOX4*-overexpression on oxylipin production in inoculated kernels

We next used ultra-HPLC-Q-TOF-MS analysis under a fully untargeted approach as previously reported by Righetti *et al.* (2021)

Downloaded from https://academic.oup.com/jxb/article/77/2/668/8271264 by guest on 13 May 2026

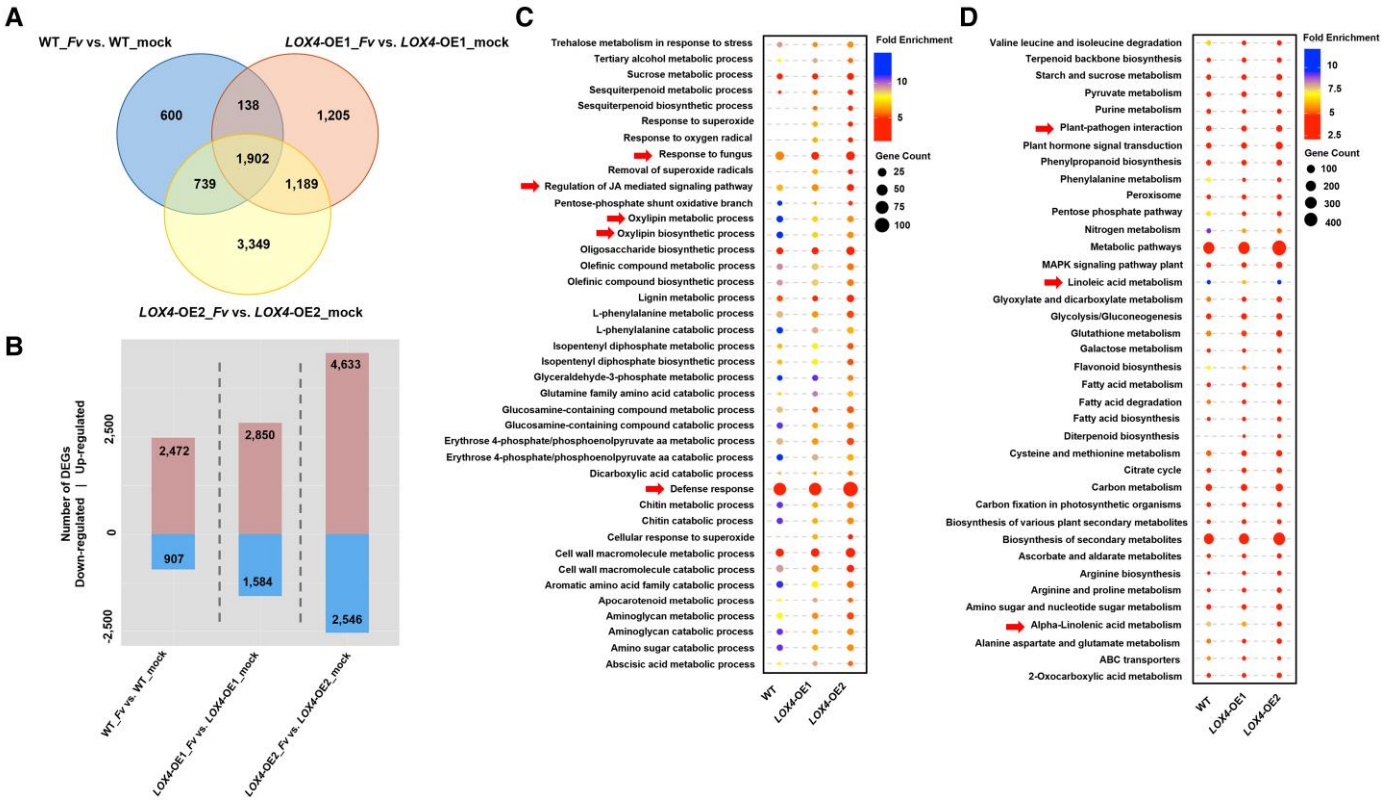


Fig. 4. RNA-seq analysis of the maize A188 wild type (WT) and two *LOX4*-overexpressing lines (OE1, OE2) following inoculation with *Fusarium verticillioides* (*Fv*) or a control solution (mock). (A) Venn diagram of the numbers of differentially expressed genes (DEGs) in comparisons of inoculated versus mock treatments within each genotype. (B) Numbers of up- and down-regulated DEGs in the three comparisons. (C) Enrichment of DEGs significantly enriched in GO term category 'Biological Process' in the three comparisons, and (D) significantly enriched KEGG pathways of DEGs in the three comparisons. The arrows highlight terms associated with defense responses and oxylipin metabolism. The size of the dots is proportional to the counts of genes, and the color indicates the fold-enrichment values as calculated by ShinyGO. The DEGs were selected according to a FDR-corrected *P*-values <0.05.

to determine which oxylipins were responsible for the enhanced resistance to *F. verticillioides* in the transgenic OE lines. Mock- and fungal-inoculated kernels at 3 dpi and 7 dpi were sampled and the raw data were subjected to principal component (PC) analysis (Fig. 5A–C). PC1 and PC2 were selected as linear combinations to represent the variability of the overall dataset. The analysis revealed a clear separation between the mock and inoculated samples for all three genotypes. Intriguingly, the inoculated samples at the two sampling dates from both the OE lines were more distinctly separated from the control compared with the WT, indicating that multiple oxylipins could contribute to FER resistance.

A total of 31 compounds were annotated as showing different accumulation patterns in the three genotypes (Fig. 5D; Supplementary Table S8.1). For the majority of oxylipins, a lower content was measured in the mock-treated kernels of the transgenic genotypes, mainly at 3 dpi, in comparison with the WT, consistent with the higher numbers of down-regulated 9- and 13-LOX genes observed at the basal level (Fig. 3C; Supplementary Table S8.2). At 3 dpi in the *F. verticillioides* treatment, all the oxylipins that were induced were always more strongly affected in the transgenic lines, in particular in OE2, with the exception of 13-oxoODE. The highest $\log_2$-FC values were found for traumatic acid (13-LOX), with values of 8.26, 10.53, and 9.81 for the WT, OE1, and OE2, respectively. At 7 dpi, in most cases in the WT an increase of compound concentrations was observed, whereas values declined in the OE lines, excluding the oxylipins 12-EpOME and 13-HOTre that continued to maintain elevated levels in all three genotypes.

Overall, these results indicated that increased expression of *LOX4* led to the greater production of both key 9- and 13-oxylipins, mainly at the early infection stage. This higher oxylipin content might be responsible for the enhanced resistance to *F. verticillioides* observed in *LOX4*-OE kernels.

Effects of *LOX4*-overexpression on phytohormone contents kernels in response to infection

Phytohormones, particularly jasmonates and salicylic acid, are key signaling molecules that are active during plant–pathogen interactions. Therefore, we next examined changes in their concentrations in kernels of the WT and OE lines at 3 dpi

Downloaded from https://academic.oup.com/jxb/article/77/2/668/8271264 by guest on 13 May 2026

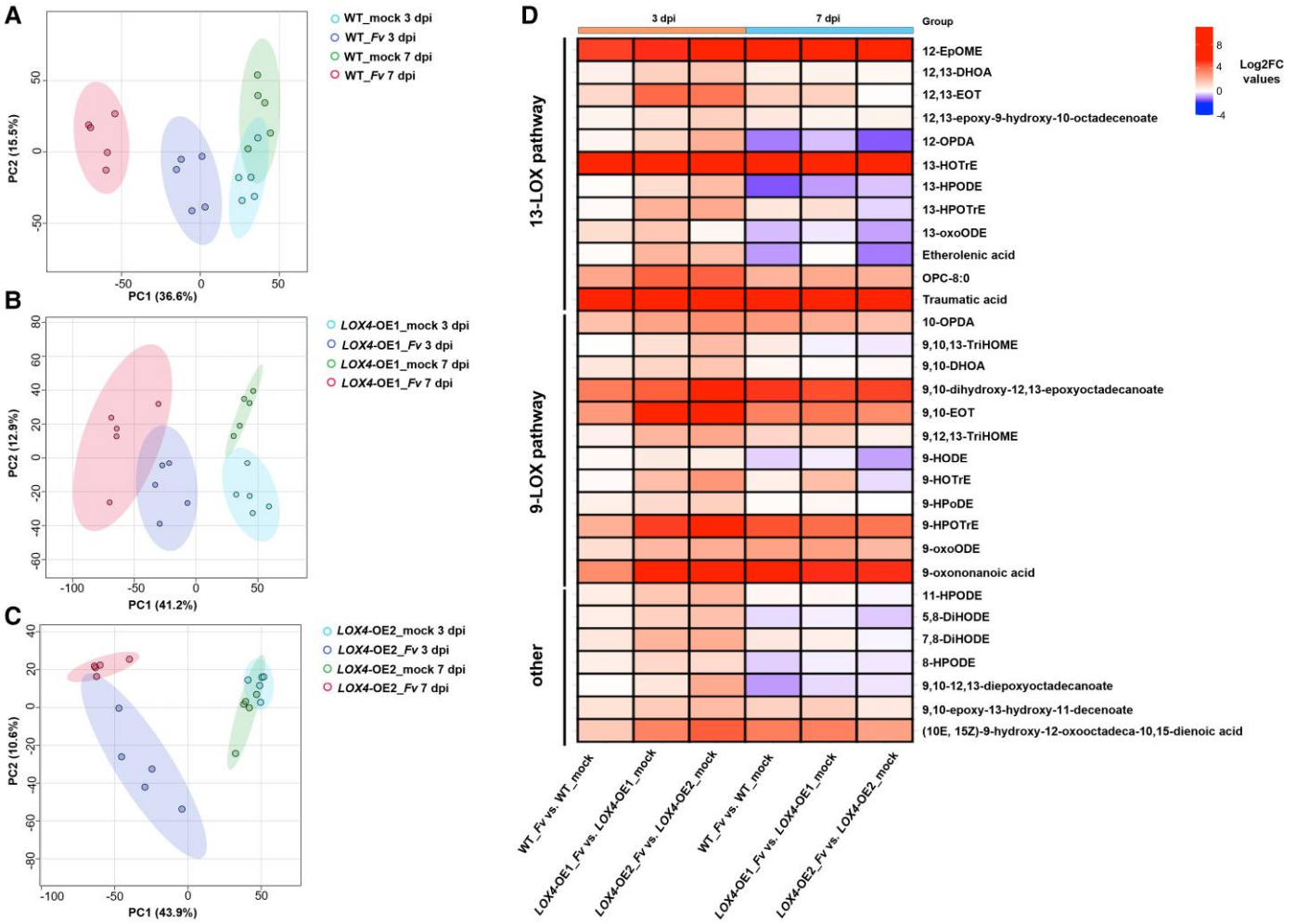


Fig. 5. Oxylipin profiling of the maize A188 wild type (WT) and two *LOX4*-overexpressing lines (OE1, OE2) at 3 days post inoculation (dpi) and 7 dpi with *Fusarium verticillioides* (*Fv*) or a control solution (mock). (A–C) Principal component (PC) analysis of the raw data for (A) the WT, (B) OE1, and (C) OE2 based on the oxylipin profiling of five replicate samples for each the three genotypes. PC1 and PC2 have been selected as linear combinations to represent the variability of the overall dataset. (D) Heat-map of significantly modulated oxylipins in the 9- and 13-LOX and other pathways for the comparisons of infected versus mock treatments within each genotype at 3 dpi and 7 dpi.

and 7 dpi with mock and *F. verticillioides* treatments. In addition to JA and SA, we also examined the JA biosynthetic precursor 12-oxophytodienoic acid (*cis*-OPDA), the bioactive jasmonoyl isoleucine conjugate (JA-Ile), and inactive hydroxylated and carboxylated degradation metabolites. The results showed that at 3 dpi in the mock treatment both the OE lines had significantly reduced constitutive concentrations of SA compared to the WT (Fig. 6A). In the inoculated treatment at 3 dpi, there was a significant increase in concentration in OE2 compared with the mock. Infection had no significant effect at 7 dpi.

For the jasmonates, the concentrations of *cis*-OPDA, JA, and its derivatives were in most cases lower in the mock-treated kernels of the OE lines than in the WT at both stages, with the exception of JA-Ile at 7 dpi (Fig. 6E). This was consistent with the results of the RNA-seq analysis, at least at the early infection stage, where widespread down-regulation of genes involved in the JA-mediated signaling pathway was observed in the two OE lines (Fig. 3C).

Inoculation with *F. verticillioides* triggered significant increases for most JA-related metabolites independently of the genotype, apart from *cis*-OPDA at 7 dpi (Fig. 6B–G). JA-Ile showed the highest concentrations following infection with values of 257.5, 142.0, and 227.4 ng g^{-1} FW for the WT, OE1, and OE2, respectively, followed by JA and OH-JA. Notably, in terms of the ratio in concentrations between the fungal- and mock-inoculated treatments, the increment was more pronounced in the OE lines for the majority of compounds. In particular, OE2 always showed the highest increase, ranging from ~5 times for OH-JA-Ile at 7 dpi (compared with 2.7 for the WT) to ~79 times for COOH-JA-Ile at 3 dpi (4.5 for the WT). Taken together, these results further reinforce the involvement of JA as a regulator of defense against

Downloaded from https://academic.oup.com/jxb/article/77/2/668/8271264 by guest on 13 May 2026

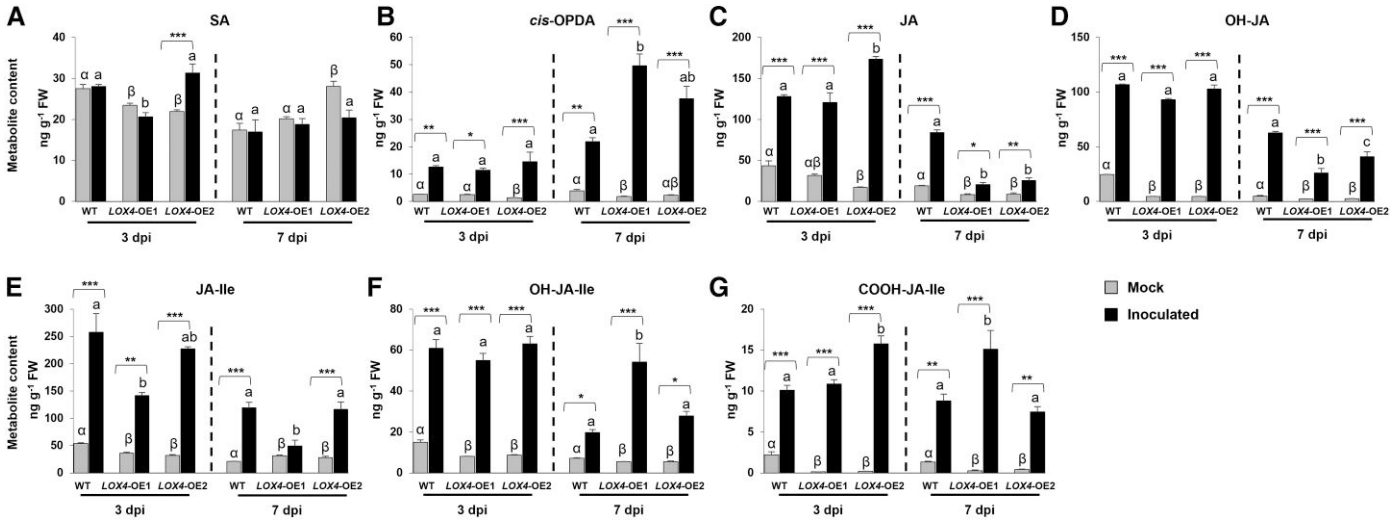


Fig. 6. Hormone profiling of the maize A188 wild type (WT) and two *LOX4*-overexpressing lines (OE1, OE2) at 3 days post inoculation (dpi) and 7 dpi with *Fusarium verticillioides* or a control solution (mock). (A) Salicylic acid (SA), (B)12-oxo-phytodienoic acid (*cis*-OPDA), (C) jasmonic acid (JA), (D) 12-hydroxyjasmonic acid, OH-JA, (E) jasmonoyl isoleucine conjugate (JA-Ile), (F) hydroxyjasmonoyl-isoleucine (OH-JA-Ile), and (G) COOH-JA-Ile (dicarboxyjasmonoyl-isoleucine). Data are means (±SD), n=3. Different letters indicate significant differences among means as determined using one-way ANOVA followed by Tukey's HSD test (P<0.05), with Greek letters being used for differences among the mock treatments. Significant differences between the mock and inoculated treatments within a genotype were determined using two-way ANOVA: *P≤0.05, **P≤0.01, ***P≤0.001.

F. verticillioides and highlight that *LOX4*-overexpression positively matched with a wider activity in the JA biosynthetic pathway, which was especially clear in the strong *LOX4*-OE2 line.

Multi-omics analysis of *LOX4* expression and *F. verticillioides* infection

The combined analysis of the transcriptome and 9- and 13-oxylipin profiling in the WT and *LOX4*-OE genotypes at 3 dpi and 7 dpi with *F. verticillioides* are shown in Fig. 7. In the 13-LOX pathway, the majority of the compounds involved in JA biosynthesis were produced at higher levels in the infected OE lines at 3 dpi (Fig. 7A), including 13-HOTrE, 12-OPDA, OPC-8:0, JA, and JA derivatives, especially COOH-JA-Ile. In line with these results, the key genes encoding enzymes catalysing the formation of JA precursors showed higher expression in the OE lines, such as *13-LOXs*, *AOS1c*, *AOC1*, *OPR1-5*, *OPC1*, *ACX* and *acetyl C*. Moreover, most of the genes for CYP94 isoforms that convert JA-Ile to OH-JA-Ile and COOH-JA-Ile showed a similar trend.

Quantification of 9-oxylipins identified 9-oxononanoic acid followed by 9-HPOTrE as the most induced compounds for the OE lines at 3 dpi (Fig. 7B), and this was reflected by increases in the 9-oxylipins produced by the 9-POX, 9-AOS, and EAS/EAH branch pathways. 9-LOX genes including *LOX1*, *LOX2*, and *LOX3* were specifically induced in the OE2 line, and the death acid-producing genes *AOS1a* and *AOS2b* also exhibited higher expression levels in the OE lines, consistent with the 9-oxylipin accumulation results.

To confirm the role of 9- and 13-oxylipins as antifungal agents, we grew cultures of *F. verticillioides* for 7 d at 25 °C in presence of 12-OPDA, *trans*-2-hexenal, JA, traumatic acid, or 9-oxononanoic acid, and found that the area under the growth curves was significantly reduced by the presence of all the compounds (Supplementary Fig. S11), confirming the contribution of these oxylipins to pathogen resistance.

Discussion

Plant diseases provoked by pathogens result in significant reductions in yield and quality of important crops annually across the world (Gai and Wang, 2024). *Fusarium* spp. can cause considerable injury to a wide range of tissues in maize, most notably in terms of ear, stalk, and seedling rot (Gai *et al.*, 2018). Ear rot caused by *F. verticillioides* is the most common fungal disease on corn ears, and the development of durable genetic resistance is becoming a more and more pressing concern to contain its spread. Lipoxygenases play critical roles in plant responses to pathogen attack (Viswanath *et al.*, 2020), and it has been demonstrated that oxylipins synthetized by the LOX pathway possess antimicrobial properties and/or act as signaling molecules in plant defense systems (Feussner and Wasternack, 2002; Christensen *et al.*, 2015; Sugimoto *et al.*, 2022). In our previous studies, we have examined the effects of LOXs against *F. verticillioides* in maize through the use of mutants carrying *Mu* transposon insertions in *LOX4*. Gene mutagenesis impairs fungal resistance, reshapes the expression of *LOX*s, and alters oxylipin profiles at different plant developmental stages in kernels (Battilani *et al.*, 2018), seedlings (Lanubile *et al.*, 2021a), and

Downloaded from https://academic.oup.com/jxb/article/77/2/668/8271264 by guest on 13 May 2026

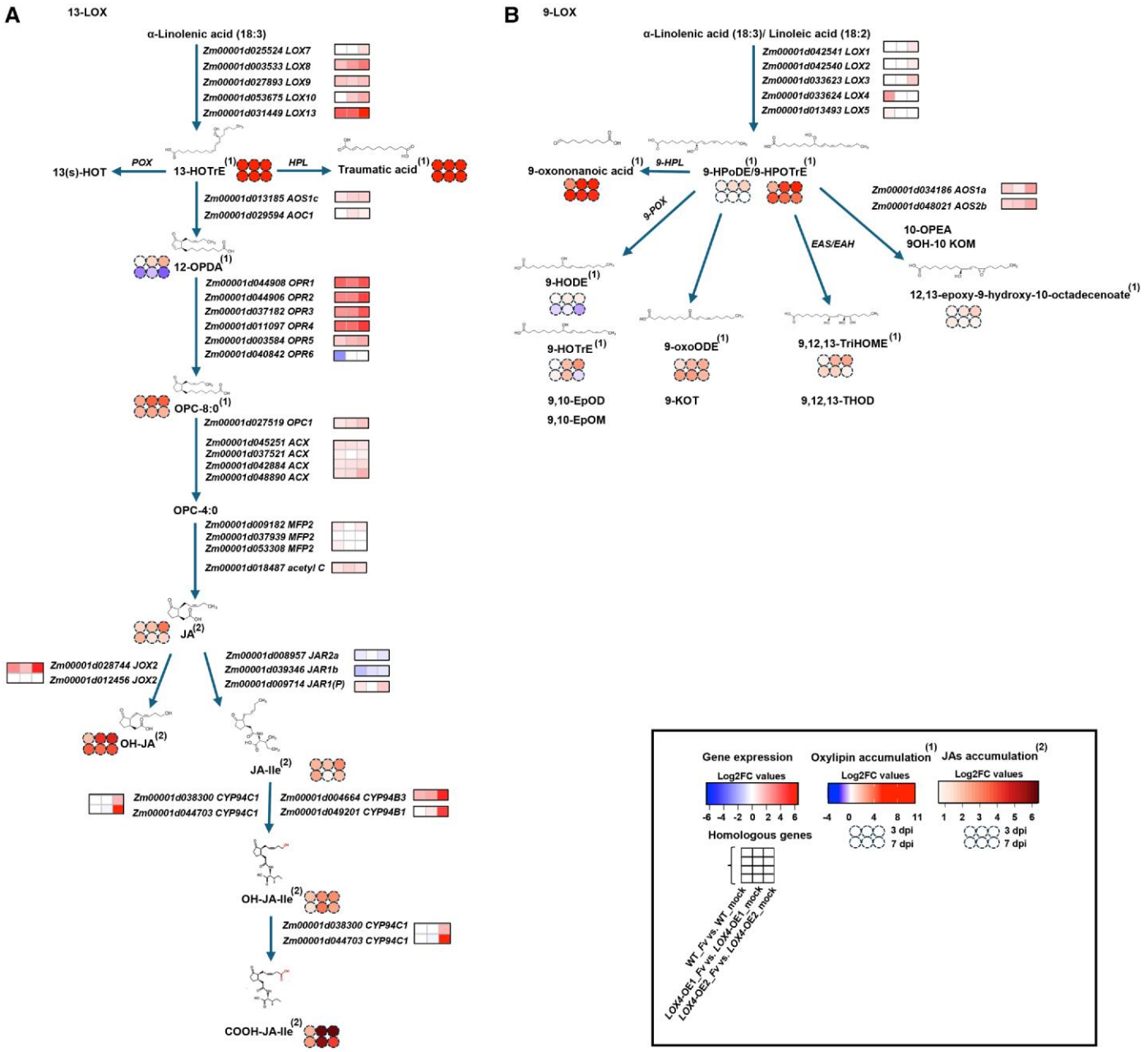


Fig. 7. Activation of the 13- and 9-LOX pathways in response to *Fusarium verticillioides* (*Fv*) in the maize A188 wild type (WT) and two *LOX4*-overexpressing lines (OE1, OE2) at 3 days post inoculation (dpi) and 7 dpi with *Fusarium verticillioides* (*Fv*) or a control solution (mock). (A) The 13-LOX pathway and (B) the 9-LOX pathway. The presentation of the heat-maps is described in the key, and the colors represent the $\log_2$(fold-change) in gene expression for each comparison (Supplementary Table S6). Circles represent the $\log_2$(fold-change) of oxylipin/hormone content for each comparison (Supplementary Table S8). (1) and (2) represent compounds derived from the untargeted lipidomics and hormone profiling analyses, respectively.

ears (Guche *et al.*, 2022). There have been several studies on the genetic manipulation of *LOX*s both in monocots (Zabbai *et al.*, 2004; Sharma *et al.*, 2006; Cho *et al.*, 2012; Losvik *et al.*, 2017; Liao *et al.*, 2022) and dicots (Hwang and Hwang, 2010; Hu *et al.*, 2013; Hou *et al.*, 2018; Tolley *et al.*, 2023; Xu *et al.*, 2024), but in this current study we describe for the first time the effects of constitutive overexpression of *LOX4* in transgenic maize. Our results showed that transgenic *LOX4*-OE maize plants displayed increased resistance to *F. verticillioides* ear rot (FER) as well as a lower fumonisin content (Fig. 2). In addition, reduced scores for severity of *F. verticillioides* seedling rot (FSR) and fungal biomass levels were observed in the OE lines. Interestingly, in the absence of infection, plant height, ear length, kernel number per ear, and

Downloaded from https://academic.oup.com/jxb/article/77/2/668/8271264 by guest on 13 May 2026

100-grain weight were not affected by the overexpression of *LOX4* (Supplementary Fig. S3). However, it was apparent that at the seedling stage there were increases in seedling weight and length in the OE lines (Supplementary Fig. S4), particularly in OE2, which had the highest levels of *LOX4* transcripts (Fig. 1), suggesting it had possible effects in the development process. Previous studies have reported the activation of several LOXs aimed at lipid mobilizing during the early stage of seedling growth in different species, including Arabidopsis, *Vigna radiata*, *Citrullus lanatus*, *Oryza sativa*, and *Brassica napus* (see Singh *et al.*, 2022), and up-regulation of genes encoding 9-LOXs has been observed throughout seed maturation in almond and maize (Jensen *et al.*, 1997; Santino *et al.*, 2005). In addition, JA catabolism has been shown to be crucial to sex determination and plant architecture in both rice and maize crops (Lunde *et al.*, 2019; Wang *et al.*, 2020). It still remains a challenge to elucidate the interactions among various oxylipin signaling pathways during the life cycle of a plant under different stress conditions that result in reduced development.

Overexpression of *LOX4* led to remodeling of the transcriptome both with and without *F. verticillioides* infection. At the basal level, there was a general down-regulation of 9- and 13-LOX genes (Fig. 3) that was accompanied by lower contents of oxylipins and jasmonates (Fig. 5). Following fungal inoculation, substantial transcriptional changes were found and the number of resulting DEGs was directly proportional to the expression of the transgene (Figs 1, 4B). Oxylipin profiling confirmed this trend, particularly at 3 dpi, with the highest modulation being observed for the *LOX4*-OE2 line, followed by *LOX4*-OE1 and the WT (Fig. 7).

In terms of the transcriptomic results, whilst a considerable number of defense-associated GO and KEGG terms were common between the WT and the OE lines, the level of induction was generally much higher in the overexpressing plants (Supplementary Figs S7, S8). Chitinases were highly abundant among the up-regulated genes related to defense categories. Maize chitinases display a key role in defense against fungi containing chitin in their cell walls (Kumar *et al.*, 2018), and Cazares-Álvarez *et al.* (2024) have recently reported the induction of 10 different maize chitinases in response to *F. verticillioides*, with differing roles according to their domain type and subcellular localization. Other transcriptomic studies have also highlighted the involvement of chitinase genes in the pathogen-associated molecular pattern-triggered immunity against FER in maize (Lanubile *et al.*, 2014b; Wang *et al.*, 2016).

An additional strongly enriched KEGG term in response to infection was 'Biosynthesis of secondary metabolites', including DEGs related to phenylpropanoids, flavonoids, and terpenoids/diterpenoids (Fig. 4), compounds that are well known to be associated with inhibiting fungal growth and promoting resistance to *F. verticillioides* infection. In our previous study, RNA-sequencing identified 126 DEGs attributed to the 'secondary metabolism' category in maize ears at 72 hpi, and among the most represented pathways metabolic processes associated with terpenoid synthesis were highly expressed (Lanubile *et al.*, 2014b). Similar findings were reported by Tran *et al.* (2024) who found that several hundred genes related to terpene synthesis were differentially expressed in young seedlings of eight different maize lines after *F. verticillioides* inoculation. Furthermore, a transcriptomic analysis by Lambarey *et al.* (2020) identified a gene encoding a terpene synthase (*TPS1*) as the most significantly up-regulated in infected shoot tissues, and this was associated with enhanced kauralexin accumulation.

Interestingly, overexpression of *LOX4* caused specific enrichment for the GO terms 'Response to superoxide', 'Response to oxygen radical', 'Removal of superoxide radicals', and 'Cellular response to superoxide'. Reactive oxygen species (ROS) act as signaling molecules and represent one of the earliest plant defense strategies (Jwa and Hwang, 2017; Zaid and Wani, 2019). The production of ROS by plants is mainly associated with infection by biotrophic and hemibiotrophic fungi and can culminate in localized cell death (Constantino *et al.*, 2013; McCormick, 2017). Previous studies have reported that maize *lox3* mutants show enhanced levels of ROS against *Ustilago maydis* (Pathi *et al.*, 2020) and *C. graminicola* (Constantino *et al.*, 2013), suggesting that ROS accumulation can shorten the biotrophic stage during the infection, and further indicating the possible role of lipoxygenases in the accumulation.

Our transcriptomic profiling also highlighted a widespread up-regulation of both 9-LOX- and JA-associated genes in response to *F. verticillioides*, which was correlated with increased contents and was more pronounced in the *LOX4*-OE lines (Fig. 7). It has been reported that decreased resistance to Gibberella stalk rot in maize *lox5* mutants is related to reduced contents of multiple 9-oxylipins, including 9(S)-hydroxy-10(E),12(Z),15(Z)-octadecatrienoic acid (9-HOT), 9(S)-hydroxy-10(E),12(Z)-octadecadienoic acid (9-HOD), 9-keto-10(E),12(Z),15(Z)-octadecatrienoic acid (9-KOT), 9-keto-10(E),12(Z)-octadecadienoic acid (9-KOD), 10-oxo-9-hydroxy-12(Z) and 15(Z)-octadecenoic acid (9OH-10KOM), and 10-oxo-9-hydroxy-12(Z) and 15(Z)-octadecadienoic acid (9OH-10KOD) (Wang *et al.*, 2021). In line with this, a duplicated copy-number variant of *LOX5*, a paralog of *LOX4*, results in improved resistance to herbivory by fall armyworms that is mediated by higher levels of 9-hydroxy-10-oxo-12(Z),15(Z)-octadecadienoic acid (9,10 KODA) (Yuan *et al.*, 2024). In a previous study, we observed rapid production of 9-hydroxy-10,12-octadecadienoic acid (9-HODE) and 10-oxo-11-phytoenoic acid (10-OPEA) at 3 dpi with *F. verticillioides* in two resistant maize genotypes, whereas no accumulation was found in a *lox4* mutant (Guche *et al.*, 2022). Whilst we found increased transcript levels of the putative biosynthetic genes encoding 9-allene oxide synthase *AOS1a* and *AOS2b* in the current study (Fig. 7), we did not measure 10-OPEA. Conversely, an early induction of its 13-LOX analog 12-OPDA and the associated transcripts,

Downloaded from https://academic.oup.com/jxb/article/77/2/668/8271264 by guest on 13 May 2026

AOS1c and allene oxide cyclase (*AOC1*), was observed mainly in the *LOX4*-overexpressing lines. Along with 12-OPDA, the majority of jasmonates were highly induced in the OE lines in response to *F. verticillioides* treatment, suggesting a positive correlation of JAs with improved resistance to FER. The early synthesis of JA and its derivatives was further supported by the up-regulation of genes involved in JA production and those regulated by JA, showing that 9-oxylipins produced by *LOX4*-overexpression had a large positive effect on the 13-LOX pathway after fungal treatment. The role of JA as the main defense hormone required for immunity against *F. verticillioides* is demonstrated by the JA-deficient maize *opr7 opr8* double-mutant that exhibits complete susceptibility to this pathogen (Christensen *et al.*, 2014). However, strong antagonism among JA, and 13- and 9-oxylipins is found in this double-mutant and in the *lox10* mutant, and the suppression of 13-oxylipins results in overproduction of several wound-induced 9-oxylipins (He *et al.*, 2020). Similarly, increased accumulation of 9-oxylipins in the maize *lox5* mutant has a negative effect on JA biosynthesis and on plant resistance towards *F. graminearum* (Wang *et al.*, 2021). Further studies are required to better clarify the crosstalk between JA and oxylipins, which appears to work in a pathogen-dependent manner.

In summary, this study confirms the fundamental role of *LOX4* in defense strategies against *F. verticillioides*. Overexpression of this gene not only positively affected the production of multiple 9-oxylipins via increased expression levels of 9-LOX genes but also had a cascade effect on JA contents as well as leading to higher expression of JA-related genes. This corresponded with an enhanced resistance to the pathogen and reduced fumonisin contamination. Moreover, the antimicrobial activity of the key oxylipins 12-OPDA, *trans*-2-hexenal, JA, traumatic acid, and 9-oxononanoic acid was confirmed by observations of their inhibitory effects on *F. verticillioides* growth. It will be interesting to conduct further studies to evaluate the effects of *LOX4*-overexpression on other fungi and pathogenic insects and to examine possible trade-offs. Additionally, it is our intention to explore the effects of *LOX4*-overexpression in response to abiotic stresses. In this regard, Li *et al.* (2025) observed up-regulation of *LOX4* in response to heat, drought, and cold stresses, suggesting that it could provide a new target for enhancing maize resilience to different environmental conditions.

Supplementary data

The following supplementary data are available at *JXB* online.

Fig. S1. Schematic overview of experimental timeline.

Fig. S2. Representative images of non-infected plants for the WT, *LOX4*-OE1, and *LOX4*-OE2 at week 8.

Fig. S3. Plant height, ear, and kernel measurements for non-infected plants of the three genotypes.

Fig. S4. Seedling weights and lengths for the three genotypes at 7 dpi with and without *F. verticillioides*.

Fig. S5. Distribution of RNA-seq reads across introns, exons, UTRs, and intergenic regions for each of the different treatments.

Fig. S6. Expression heat-maps and clustering of differentially expressed genes into 6 groups based on the expression profiles.

Fig. S7. Bubble-plots showing enriched GO terms classified as 'Biological Process' in differentially expressed genes in comparisons of mock-inoculated genotypes.

Fig. S8. Bubble-plots showing enriched KEGG pathways in differentially expressed genes in comparisons of mock-inoculated genotypes.

Fig. S9. Expression heat-map of DEGs involved in the 9- and 13-LOX pathways, and the JA-mediated signaling pathway in the three genotypes following *F. verticillioides* inoculation.

Fig. S10.Validation of the RNA-seq results by RT-qPCR analysis.

Fig. S11. Area under the growth curve of cultures of *F. verticillioides* subjected to treatment with different 9- and 13-oxylipins.

Table S1. Primer sequences for PCR and RT-qPCR analyses.

Table S2. Cq values of the *actin* reference gene under all experimental conditions.

Table S3. Summary statistics of paired-end sequenced reads produced and aligned with the *Zea mays* B73 GRAMENE v4 genome.

Table S4. Raw counts for each gene for each biological replicate for mock- and *F. verticillioides*-inoculated samples.

Table S5. Expression levels and annotations of differentially expressed genes in comparisons of mock-inoculated genotypes.

Table S6. Expression levels and annotation results of differentially expressed genes in comparisons of *F. verticillioides*-inoculated genotypes.

Table S7. GO term enrichment in 'Biological Process' and KEGG pathway enrichment of differentially expressed genes in comparisons of mock-inoculated genotypes.

Table S8. List of oxylipins identified in the three genotypes at 3 dpi and 7dpi.

Acknowledgements

The authors are thankful to Paola Battilani (Catholic University of the Sacred Heart) for kindly providing *Fusarium verticillioides* strain and to Michael Reichelt (Max Planck Institute for Chemical Ecology) for support with the phytohormone measurements. We are also thankful to Peter Rogowsky for his help in designing *ZmLOX4*-OE lines and his constant and valuable support; to Camille Knaupp, Justin Berger, Patrice Bolland, Isabelle Desbouchages, and Hervé Leyral for technical assistance with the maize cultures and media preparation; and to Cindy Vial, Laureen Grangier, Nelly Camilleri, and Julie Prata for administrative assistance (all ENS de Lyon). We are also thankful to Giovanni Maria Di Pasquale (Catholic University of the Sacred Heart) for his support with fungal growth bioassay.

Author contributions

AL and AMa conceived the study; EM and TW generated the *LOX4*-OE lines; LO, PG, CD, and AMi performed the experiments; AL, LO, and CD analysed the data; AL, LO, TW, and CD prepared the figures; AL and LO wrote the manuscript; AMa, AMi, and TW reviewed and edited the manuscript; all authors contributed to the manuscript and approved the submitted version.

Conflict of interest

The authors declare that they have no conflicts of interest in relation to this work.

Funding

LO was supported by a PhD fellowship from the Doctoral School on the Agro-Food System (Agrisystem) of Università Cattolica del Sacro Cuore (Italy), which was co-funded by Programma Operativo Nazionale

Downloaded from https://academic.oup.com/jxb/article/77/2/668/8271264 by guest on 13 May 2026

Ricerca e Innovazione 2014–2020, risorse FSE REACT-EU Azione IV.4 'Dottorati e contratti di ricerca su tematiche dell'innovazione' e Azione IV.5 'Dottorati su tematiche Green'.

Data availability

Raw sequences are available in the NCBI Sequence Read Archive (https://www.ncbi.nlm.nih.gov/sra) under BioProject accession no. PRJNA1101865.

References

Anders S, Huber W. 2010. Differential expression analysis for sequence count data. Genome Biology **11**, 106–110.

Battilani P, Lanubile A, Scala V, *et al.* 2018. Oxylipins from both pathogen and host antagonize jasmonic acid-mediated defence via the 9-lipoxygenase pathway in *Fusarium verticillioides* infection of maize. Molecular Plant Pathology **19**, 2162–2176.

Berens ML, Berry HM, Mine A, Argueso CT, Tsuda K. 2017. Evolution of hormone signaling networks in plant defense. Annual Review of Phytopathology **55**, 401–425.

Berg-Falloure KM, Kolomiets MV. 2023. Ketols emerge as potent oxylipin signals regulating diverse physiological processes in plants. Plants **12**, 2088.

Borrego EJ, Kolomiets MV. 2016. Synthesis and functions of jasmonates in maize. Plants **5**, 41.

Camardo Leggieri M, Lanubile A, Dall'Asta C, Pietri A, Battilani P. 2020. The impact of seasonal weather variation on mycotoxins: maize crop in 2014 in northern Italy as a case study. World Mycotoxin Journal **13**, 25–36.

Cazares-Álvarez JE, Báez-Astorga PA, Arroyo-Becerra A, Maldonado-Mendoza IE. 2024. Genome-wide identification of a maize chitinase gene family and the induction of its expression by *Fusarium verticillioides* (Sacc.) Nirenberg (1976) infection. Genes **15**, 1087.

Cho K, Kim YC, Woo JC, Rakwal R, Agrawal GK, Yoeun S, Han O. 2012. Transgenic expression of dual positional maize lipoxygenase–1 leads to the regulation of defense–related signaling molecules and activation of the antioxidative enzyme system in rice. Plant Science **185–186**, 238–245.

Christensen SA, Nemchenko A, Park Y-S, *et al.* 2014. The novel monocot-specific 9-lipoxygenase *ZmLOX12* is required to mount an effective jasmonate-mediated defense against *Fusarium verticillioides* in maize. Molecular Plant-Microbe Interaction **27**, 1263–1276.

Christensen SA, Huffaker A, Kaplan F, *et al.* 2015. Maize death acids, 9-lipoxygenase-derived cyclopente(a)nones, display activity as cytotoxic phytoalexins and transcriptional mediators. Proceedings of the National Academy of Sciences, USA **112**, 11407–11412.

Ciasca B, Lanubile A, Marocco A, Pascale M, Logrieco AF, Lattanzio VMT. 2020. Application of an integrated and open-source workflow for LC-HRMS plant metabolomics studies. Case-control study: metabolic changes of maize in response to *Fusarium verticillioides* infection. Frontiers in Plant Science **11**, 664.

Constantino NN, Mastouri F, Damarwinasis R, Borrego EJ, Moran-Diez ME, Kenerley CM, Gao X, Kolomiets MV. 2013. Root-expressed maize lipoxygenase 3 negatively regulates induced systemic resistance to *Colletotrichum graminicola* in shoots. Frontiers in Plant Science **4**, 510.

Dávila-Lara A, Rahman-Soad A, Reichelt M, Mithöfer A. 2021. Carnivorous *Nepenthes* × *ventrata* plants use a naphthoquinone as phytoanticipin against herbivory. PLoS ONE **16**, e0258235.

Del Fabbro C, Scalabrin S, Morgante M, Giorgi FM. 2013. An extensive evaluation of read trimming effects on Illumina NGS data analysis. PLoS ONE **8**, e85024.

Dobin A, Davis CA, Schlesinger F, Drenkow J, Zaleski C, Jha S, Batut P, Chaisson M, Gingeras TR. 2013. STAR: ultrafast universal RNA-seq aligner. Bioinformatics **29**, 15–21.

Doll NM, Gilles LM, Gérentes MF, *et al.* 2019. Single and multiple gene knockouts by CRISPR–Cas9 in maize. Plant Cell Reports **38**, 487–501.

European Commission. 2007. Commission regulation No 1126/2007 amending regulation (EC) No1881/2006 setting maximum levels for certain contaminants in foodstuffs as regards Fusarium toxins in maize and maize products. Official Journal of the European Union **L255**, 14–17.

Feussner I, Wasternack C. 2002. The lipoxygenase pathway. Annual Review of Plant Biology **53**, 275–297.

Fierlej Y, Jacquier NMA, Guille L, *et al.* 2022. Evaluation of genome and base editing tools in maize protoplasts. Frontiers in Plant Science **13**, 1010030.

Gai X, Dong H, Wang S, Liu B, Zhang Z, Li X, Gao Z. 2018. Infection cycle of maize stalk rot and ear rot caused by *Fusarium verticillioides*. PLoS ONE **13**, e0201588.

Gai Y, Wang H. 2024. Plant disease: a growing threat to global food security. Agronomy **14**, 1615.

Gao X, Stumpe M, Feussner I, Kolomiets MV. 2008. A novel plastidial lipoxygenase of maize (*Zea mays*) *ZmLOX6* encodes for a fatty acid hydroperoxide lyase and is uniquely regulated by phytohormones and pathogen infection. Planta **227**, 491–503.

Gao XQ, Shim WB, Gobel C, Kunze S, Feussner I, Meeley R, Balint-Kurti P, Kolomiets M. 2007. Disruption of a maize 9-lipoxygenase results in increased resistance to fungal pathogens and reduced levels of contamination with mycotoxin fumonisin. Molecular Plant-Microbe Interactions **20**, 922–933.

Ge SX, Jung D, Yao R. 2020. ShinyGO: a graphical gene-set enrichment tool for animals and plants. Bioinformatics **36**, 2628–2629.

Gerdes JT, Tracy WF. 1993. Pedigree diversity within the Lancaster Surecrop heterotic group of maize. Crop Science **33**, 334–337.

Guche MD, Pilati S, Trenti F, Dalla Costa L, Giorni P, Guella G, Marocco A, Lanubile A. 2022. Functional study of lipoxygenase-mediated resistance against *Fusarium verticillioides* and *Aspergillus flavus* infection in maize. International Journal of Molecular Sciences **23**, 10894.

He Y, Borrego EJ, Gorman Z, Huang PC, Kolomiets MV. 2020. Relative contribution of LOX10, green leaf volatiles and JA to wound-induced local and systemic oxylipin and hormone signature in *Zea mays* (maize). Phytochemistry **174**, 112334.

Heyer M, Reichelt M, Mithöfer A. 2018. A holistic approach to analyze systemic jasmonate accumulation in individual leaves of Arabidopsis rosettes upon wounding. Frontiers in Plant Science **9**, 1569.

Hou Y, Ban Q, Meng K, He Y, Han S, Jin M, Rao J. 2018. Overexpression of persimmon 9-lipoxygenase *DkLOX3* confers resistance to *Pseudomonas syringae* pv. tomato DC3000 and *Botrytis cinerea* in Arabidopsis. Plant Growth Regulation **84**, 179–189.

Hu T, Zeng H, Hu Z, Qv X, Chen G. 2013. Overexpression of the tomato 13-lipoxygenase gene *TomloxD* increases generation of endogenous jasmonic acid and resistance to *Cladosporium fulvum* and high temperature. Plant Molecular Biology Reporter **31**, 1141–1149.

Huang PC, Tate M, Berg-Falloure KM, Christensen SA, Zhang J, Schirawski J, Meeley R, Kolomiets MV. 2023. A non-JA producing oxophytodienoate reductase functions in salicylic acid-mediated antagonism with jasmonic acid during pathogen attack. Molecular Plant Pathology **24**, 725–741.

Hwang IS, Hwang BK. 2010. The pepper 9-lipoxygenase gene *CaLOX1* functions in defense and cell death responses to microbial pathogens. Plant Physiology **152**, 948–967.

Ishida Y, Hiei Y, Komari T. 2007. *Agrobacterium*-mediated transformation of maize. Nature Protocols **2**, 1614–1621.

Jensen AB, Poca E, Rigaud M, Freyssinet G, Pagès M. 1997. Molecular characterization of L2 lipoxygenase from maize embryos. Plant Molecular Biology **33**, 605–614.

Jwa N-S, Hwang BK. 2017. Convergent evolution of pathogen effectors toward reactive oxygen species signaling networks in plants. Frontiers in Plant Science **8**, 1687.

Downloaded from https://academic.oup.com/jxb/article/77/2/668/8271264 by guest on 13 May 2026

Kanehisa M, Furumichi M, Sato Y, Ishiguro-Watanabe M, Tanabe M. 2021. KEGG: integrating viruses and cellular organisms. Nucleic Acids Research **49**, D545–D551.

Karimi M, Depicker A, Hilson P. 2007. Recombinational cloning with plant Gateway vectors. Plant Physiology **145**, 1144–1154.

Kumar M, Brar A, Yadav M, Chawade A, Vivekanand V, Pareek N. 2018. Chitinases–potential candidates for enhanced plant resistance towards fungal pathogens. Agriculture **8**, 88.

Lambarey H, Moola N, Veenstra A, Murray S, Suhail Rafudeen M. 2020. Transcriptomic analysis of a susceptible African maize line to *Fusarium verticillioides* infection. Plants **9**, 1112.

Lanubile A, Logrieco A, Battilani P, Proctor RH, Marocco A. 2013. Transcriptional changes in developing maize kernels in response to fumonisin-producing and nonproducing strains of *Fusarium verticillioides*. Plant Science **210**, 183–192.

Lanubile A, Maschietto V, Marocco A. 2014a. Breeding maize for resistance to mycotoxins. In: Leslie JF, Logrieco AF, eds. Mycotoxin reduction in grain chains. Oxford, UK: Wiley Blackwell, 37–58.

Lanubile A, Ferrarini A, Maschietto V, Delledonne M, Marocco A, Bellin D. 2014b. Functional genomic analysis of constitutive and inducible defense responses to *Fusarium verticillioides* infection in maize genotypes with contrasting ear rot resistance. BMC Genomics **15**, 710.

Lanubile A, Maschietto V, Borrelli VM, Stagnati L, Logrieco AF, Marocco A. 2017. Molecular basis of resistance to Fusarium ear rot in maize. Frontiers in Plant Science **8**, 1774.

Lanubile A, Borrelli VMG, Soccio M, Giorni P, Stagnati L, Busconi M, Marocco A. 2021a. Loss of *ZmLIPOXYGENASE4* decreases *Fusarium verticillioides* resistance in maize seedlings. Genes **12**, 335.

Lanubile A, Giorni P, Bertuzzi T, Marocco A, Battilani P. 2021b. *Fusarium verticillioides* and *Aspergillus flavus* co-occurrence influences plant and fungal transcriptional profiles in maize kernels and *in vitro*. Toxins **13**, 680.

Li S, Hou S, Sun Y, *et al.* 2025. Genome-wide identification and expression analysis under abiotic stress of the lipoxygenase gene family in maize (*Zea mays*). Genes **16**, 99.

Liao Z, Wang L, Li C, Cao M, Wang J, Yao Z, Zhou S, Zhou G, Zhang D, Lou Y. 2022. The lipoxygenase gene *OsRCI-1* is involved in the biosynthesis of herbivore-induced JAs and regulates plant defense and growth in rice. Plant, Cell & Environment **45**, 2827–2840.

Liu C, Kong M, Zhu J, Qi X, Duan C, Xie C. 2022. Engineering null mutants in *ZmFER1* confers resistance to ear rot caused by *Fusarium verticillioides* in maize. Plant Biotechnology Journal **20**, 2045–2047.

Logrieco A, Battilani P, Leggieri MC, *et al.* 2021. Perspectives on global mycotoxin issues and management from the MycoKey Maize Working Group. Plant Disease **105**, 525–537.

Losvik A, Beste L, Glinwood R, Ivarson E, Stephens J, Zhu L-H, Jonsson L. 2017. Overexpression and down-regulation of barley lipoxygenase *LOX2.2* affects jasmonate-regulated genes and aphid fecundity. International Journal of Molecular Science **18**, 2765.

Love MI, Huber W, Anders S. 2014. Moderated estimation of fold change and dispersion for RNA-seq data with DESeq2. Genome Biology **15**, 550.

Lunde C, Kimberlin A, Leiboff S, Koo AJ, Hake S. 2019. *Tasselseed5* overexpresses a wound-inducible enzyme, *ZmCYP94B1*, that affects jasmonate catabolism, sex determination, and plant architecture in maize. Communications Biology **2**, 114.

Luo W, Brouwer C. 2013. Pathview: an R/Bioconductor package for pathway-based data integration and visualization. Bioinformatics **29**, 1830–1831.

Ma P, Liu E, Zhang Z, Li T, Zhou Z, Yao W, Chen J, Wu J, Xu Y, Zhang H. 2023. Genetic variation in *ZmWAX2* confers maize resistance to *Fusarium verticillioides*. Plant Biotechnology Journal **21**, 1812–1826.

Maschietto V, Marocco A, Malachova A, Lanubile A. 2015. Resistance to *Fusarium verticillioides* and fumonisin accumulation in maize inbred lines involves an earlier and enhanced expression of lipoxygenase (*LOX*) genes. Journal of Plant Physiology **188**, 9–18.

Maschietto V, Lanubile A, De Leonardis S, Marocco A, Paciolla C. 2016. Constitutive expression of pathogenesis-related proteins and antioxidant enzyme activities triggers maize resistance towards *Fusarium verticillioides*. Journal of Plant Physiology **200**, 53–61.

Maschietto V, Colombi C, Pirona R, Pea G, Strozzi F, Marocco A, Rossini L, Lanubile A. 2017. QTL mapping and candidate genes for resistance to Fusarium ear rot and fumonisin contamination in maize. BMC Plant Biology **17**, 20.

McCormick S. 2017. Chloroplast-targeted antioxidant protein protects against necrotrophic fungal attack. Plant Journal **92**, 759–760.

Monaghan J, Zipfel C. 2012. Plant pattern recognition receptor complexes at the plasma membrane. Current Opinion in Plant Biology **15**, 349–357.

Ogunola OF, Hawkins LK, Mylroie E, Kolomiets MV, Borrego E, Tang JD, Williams WP, Warburton ML. 2017. Characterization of the maize lipoxygenase gene family in relation to aflatoxin accumulation resistance. PLoS ONE **12**, e0181265.

Pathi KM, Rink P, Budhagatapalli N, Betz R, Saado I, Hiekel S, Becker M, Djamei A, Kumlehn J. 2020. Engineering smut resistance in maize by site-directed mutagenesis of *LIPOXYGENASE 3*. Frontiers in Plant Science **11**, 543895.

Pertea M, Pertea G, Antonescu C, Chang TC, Mendell JT, Salzberg SL. 2015. StringTie enables improved reconstruction of a transcriptome from RNA-seq reads. Nature Biotechnology **33**, 290–295.

Pimentel D, Amaro R, Erban A, Mauri N, Soares F, Rego C, Martínez-Zapater JM, Mithöfer A, Kopka J, Fortes AM. 2021. Transcriptional, hormonal, and metabolic changes in susceptible grape berries under powdery mildew infection. Journal of Experimental Botany **72**, 6544–6569.

Porta H, Rocha-Sosa M. 2002. Plant lipoxygenases. Physiological and molecular features. Plant Physiology **130**, 15–21.

Righetti L, Dall'Asta C, Lucini L, Battilani P. 2021. Lipid signaling modulates the response to fumonisin contamination and its source, *Fusarium verticillioides*, in maize. Frontiers in Plant Science **12**, 701680.

Righetti L, Vanara F, Bruni R, Sardella C, Blandino M, Dall'Asta C. 2024. Investigating metabolic plant response toward deoxynivalenol accumulation in four winter cereals. Journal of Agriculture and Food Chemistry **72**, 3200–3209.

Rubert J, Righetti L, Stranska-Zachariasova M, Dzuman Z, Chrpovac J, Dall'Asta C, Hajslovaa J. 2017. Untargeted metabolomics based on ultra-high-performance liquid chromatography-high-resolution mass spectrometry merged with chemometrics: a new predictable tool for an early detection of mycotoxins. Food Chemistry **224**, 423–431.

Santino A, Iannacone R, Hughes R, Casey R, Mita G. 2005. Cloning and characterization of an almond 9-lipoxygenase expressed early during seed development. Plant Science **168**, 699–706.

Schmittgen TD, Livak KJ. 2008. Analyzing real-time PCR data by the comparative C_T method. Nature Protocols **3**, 1101–1108.

Schymanski EL, Jeon J, Gulde R, Fenner K, Ruff M, Singer HP, Hollender J. 2014. Identifying small molecules via high resolution mass spectrometry: communicating confidence. Environmental Science & Technology **48**, 2097–2098.

Septiani P, Lanubile A, Stagnati L, Busconi M, Nelissen H, Pè ME, Dell'Acqua M, Marocco A. 2019. Unravelling the genetic basis of Fusarium seedling rot resistance in the MAGIC maize population: novel targets for breeding. Scientific Reports **9**, 5665.

Sharma VK, Monostori T, Gobel C, Hansch R, Bittner F, Wasternack C, Feussner I, Mendel RR, Hause B, Schulze J. 2006. Transgenic barley plants overexpressing a 13-lipoxygenase to modify oxylipin signature. Phytochemistry **67**, 264–276.

Singh P, Arif Y, Miszczuk E, Bajguz A, Hayat S. 2022. Specific roles of lipoxygenases in development and responses to stress in plants. Plants **11**, 979.

Stagnati L, Rahjoo V, Samayoa LF, Holland JB, Borrelli VMG, Busconi M, Lanubile A, Marocco A. 2020. A genome-wide association study to

Downloaded from https://academic.oup.com/jxb/article/77/2/668/8271264 by guest on 13 May 2026

understand the effect of *Fusarium verticillioides* infection on seedlings of a maize diversity panel. Genes|Genome|Genetics **10**, 1685–1696.

Sugimoto K, Allmann S, Kolomiets MV. 2022. Editorial: oxylipins: the front line of plant interactions. Frontiers in Plant Science **13**, 878765.

Tolley JP, Gorman Z, Lei J, Yeo I-C, Nagashima Y, Joshi V, Zhu-Salzman K, Kolomiets MV, Koiwa H. 2023. Overexpression of maize *ZmLOX6* in *Arabidopsis thaliana* enhances damage-induced pentyl leaf volatile emissions that affect plant growth and interaction with aphids. Journal of Experimental Botany **74**, 1990–2004.

Tran TN, Lanubile A, Marocco A, Pè ME, Dell'Acqua M, Miculan M. 2024. Transcriptome profiling of eight *Zea mays* lines identifies genes responsible for the resistance to *Fusarium verticillioides*. BMC Plant Biology **24**, 1107.

Vaughan MM, Huffaker A, Schmelz EA, *et al.* 2014. Effects of elevated [CO_2] on maize defence against mycotoxigenic *Fusarium verticillioides*. Plant, Cell & Environment **37**, 2691–2706.

Viswanath KK, Varakumar P, Pamuru RR, Basha SJ, Mehta S, Rao AD. 2020. Plant lipoxygenases and their role in plant physiology. Journal of Plant Biology **63**, 83–95.

Wang F, Yuan ZJ, Zhao ZW, Li CX, Zhang X, Liang HF, Liu YW, Xu Q, Liu HT. 2020. *Tasselseed5* encodes a cytochrome C oxidase that functions in sex determination by affecting jasmonate catabolism in maize. Journal of Integrative Plant Biology **62**, 247–255.

Wang Q, Sun Y, Wang F, Huang P-C, Wang Y, Ruan X, Ma L, Li X, Kolomiets MV, Gao X. 2021. Transcriptome and oxylipin profiling joint analysis reveals opposite roles of 9-oxylipins and jasmonic acid in maize resistance to Gibberella stalk rot. Frontiers in Plant Science **12**, 699146.

Wang Y, Zhou Z, Gao J, Wu Y, Xia Z, Zhang H, Wu J. 2016. The mechanisms of maize resistance to *Fusarium verticillioides* by comprehensive analysis of RNA-seq data. Frontiers in Plant Science **7**, 1654.

Xu L, Xu Y, Lv H, Xu Y, Wen J, Li M, Kang J, Liu Z, Yang Q, Long R. 2024. Transcriptomic analysis reveals the mechanism of *MtLOX24* in response to methyl jasmonate stress in *Medicago truncatula*. Agriculture **14**, 1076.

Yan Y, Christensen S, Isakeit T, Engelberth J, Meeley R, Hayward A, Emery RJN, Kolomiets MV. 2012. Disruption of *OPR7* and *OPR8* reveals the versatile functions of jasmonic acid in maize development and defense. The Plant Cell **24**, 1420–1436.

Yuan P, Huang P-C, Martin TK, Chappell TM, Kolomiets MV. 2024. Duplicated copy number variant of the maize 9-lipoxygenase *ZmLOX5* improves 9,10-KODA-mediated resistance to fall armyworms. Genes **15**, 401.

Zabbai F, Jarosch B, Schaffrath U. 2004. Over-expression of chloroplastic lipoxygenase *RCI1* causes *PR1* transcript accumulation in transiently transformed rice. Physiological and Molecular Plant Pathology **64**, 37–43.

Zaid A, Wani SH. 2019. Reactive oxygen species generation, scavenging and signaling in plant defense responses. In: Jogaiah S, Abdelrahman M, eds. Bioactive molecules in plant defense. Cham, Switzerland: Springer, 111–132.

Zheng Y, Wu W, Sun C, Liu H, Dou J. 2024. Occurrence and fate analysis of mycotoxins in maize during the post-harvest period. Toxins **16**, 459.

Downloaded from https://academic.oup.com/jxb/article/77/2/668/8271264 by guest on 13 May 2026